Institute of Biomechanics
Kronesgasse 5-I
8010 Graz, Austria

Master Thesis

Damage Experiments and Constitutive Modeling of Human Thoracic and Abdominal Aortic Aneurysmal Tissues

to achieve the degree of
Master of Science

Author: Franz Maier
Supervisor: David Pierce, Ph.D.
Co-Supervisor: Hannah Weisbecker, MSc.

Head of Institute: Professor Gerhard A. Holzapfel, Ph.D.

April 30, 2014

Contents

Abstract

The development and growth of an aortic aneurysm includes structural changes within the vessel wall: collagen content increases, elastin content reduces and smooth muscle cells degenerate. With this study we want to quantify the impact of these changes on the passive mechanical response of the diseased tissue by estimating appropriate material parameters via mechanical testing and constitutive modeling. This study continues the work from Weisbecker et al. (2012) and extends the usage of the anisotropic pseudo-elastic damage model to diseased thoracic and abdominal aortic tissue.
Uniaxial extension tests on circumferentially and axially oriented strips from 6 thoracic (65.6 years $\pm$ 13.4, mean $\pm$ std) and 8 abdominal (63.9 years $\pm$ 11.4) aortic fusiform aneurysms on several load steps up to the supra-physiological loading range were performed. For every load step three loading cycles were applied to observe continuous and discontinuous softening. The mechanical data was fit with the pseudo-elastic constitutive model from Weisbecker et al. (2012) to gather, in a first step material parameters and subsequently damage parameters to quantify the softening of the tissue. Using the Wilcoxon rank sum test, the significance of the differences between the fitted material parameters: diseased thoracic versus abdominal tissues and healthy (Weisbecker et al. 2012) versus diseased tissues was determined. Furthermore correlations of these parameters with age, BMI and preoperative aneurysm diameter were examined. To get additional insight in the tissue microstructure and a better understanding of the fitted material parameters, we investigated histological cuts following standard procedures, from every sample tested.
The material response was clearly anisotropic for all cases, and the constitutive model fits the data well for both the primary loading curve and the discontinuous softening which we interpret as damage. Statistically relevant differences between material parameters fitted to diseased thoracic versus abdominal tissues, as well as between those fitted to healthy versus diseased tissues, were found. Relative to healthy tissue (Weisbecker et al. 2012), softening initiates at smaller strains in diseased tissues. The histological investigation showed typical signs of remodeling of the main structural elements within the wall, with a higher characteristic in the abdominal samples.
In light of the degeneration of active cells, the mechanical properties of highly remodeled aortic aneurysmal tissues might be fully characterized with passive testing alone. Due to large patient variability many 'one criterion for all' approaches to estimate the rupture risk of aneurysms are unlikely to be accurate when applied to individuals. Future methods should tend toward patient-specific risk estimations using, e.g., finite element simulations calibrated using data such as those provided here.

Zusammenfassung

Die Entwicklung und das Wachstum von Aortenaneurysmen führt zu strukturellen Veränderungen in der Gefäßwand: der Kollagengehalt steigt, Elastin und die glatte Muskulatur werden abgebaut. Mit dieser Studie sollen die Auswirkungen dieser Änderungen auf die passiven mechanischen Eigenschaften von krankhaftem Gewebe quantifiziert werden, indem aussagekräftige Materialparameter durch mechanisches Testen und Modellieren ermittelt werden. Diese Arbeit führt die Studie von Weisbecker et al. (2012) fort und die Anwendung des pseudo-elastischen Schädigungsmodells auf krankhaftes thorakales und abdominales Aortengewebe erweitert.
An sechs thorakalen (65.6 Jahre $\pm$ 13.4, Mittelwert $\pm$ Standardabweichung.) und acht abdominalen (63.9 Jahre $\pm$ 11.4) fusiformen Aortenaneurysmen wurden uniaxiale Zugversuche in Umfangs- und Längsrichtung durchgeführt, dabei wurde die Belastung schrittweise bis in den superphysiologischen Bereich erhöht. Bei jeder Belastungsstufe wurden drei Be- und Entlastungszyklen aufgenommen um kontinuierliche und diskontinuierliche Erweichung zu beobachten. Die erhaltenen Daten wurden mit einem pseudo-elatischen Materialgesetz gefitted, um Material- und Schädigungsparameter zu erhalten. Mit dem Wilcoxon Rangsummentest wurden die Ergebnisse auf signifikante Unterschiede, sowohl zwischen gesundem und erkranktem Gewebe, als auch zwischen thorakalen und abdominalen erkranktem Gewebe untersucht. Um einen zusätzlichen Einblick in die Mikrostruktur des Gewebes zu erhalten und um die erhaltenen Materialparameter besser interpretieren zu können, wurden histologische Schnitte von allen getesteten Proben angefertigt.
Die Materialantwort war in allen Fällen eindeutig anisotrop und das Materialmodell liefert eine gute Übereinstimmung, sowohl für die Erstbelastungskurve, als auch für das diskontinuierliche Erweichen. Statistisch relevante Unterschiede in den Materialparametern wurden sowohl zwischen gesunden und kranken, als auch zwischen krankem abdominalen und thorakalen Gewebe gefunden. Verglichen mit gesundem Gewebe (Weisbecker et al. 2012) erweicht sich das erkrankte Gewebe schon bei kleineren Dehnungen. Die histologische Untersuchung zeigte typische Veränderungen im remodellierten Gewebe, die aber in den abdominalen Proben wesentlich stärker ausgeprägt waren.
In Anbetracht der Rückbildung der aktiven Komponenten, in einer stark umgebauten Aortenwand, lassen sich die mechanischen Eigenschaften hinreichend durch passives Testen beschreiben. Die großen Unterschiede zwischen den erhaltenen Materialparametern verhindern die Erstellung eines allgemein gltigen Ktiteriums, um das Risiko einer Ruptur für verschiedene Individuen anzugeben.

Acknowledgment

First of all I owe particular thanks to my parents, my mother Berta Maier and my father Franz Maier, who always supported my decisions and gave me the great opportunity to complete my studies.
Further I want to thank my Supervisors David Pierce, PhD, and Hannah Weisbecker, MSc, for their endless support and patience during the conduction of this work.
Special thanks go to the head of the Institute of Biomechanics, at the University of Technology in Graz, Gerhard Holzapfel, PhD, and all his coworkers who provided the laboratory facilities and always had a piece of good advice, when needed.
A great benefit was the support of Christian Viertler, PhD, from the Institue of Pathology at the Landeskrankenhaus Graz, with his help for the histological analysis.
I also want to express my sincere gratitude to all the members of the SCATh Team in Leuven for collecting and providing the samples that made it possible to write my thesis in the first place.
In addition, I want to thank all my student colleagues who supported me during my studies and made many things much easier during this long process of finalizing this important step in my life. Also many thanks to all my friends who devotedly distracted me for the purpose of keeping a clear head when things seemed to complicated. At this point I want to send special thanks to my long-term roommate, Christoph Latschbacher, who provided an inspiring ambiance, both for my studies and the 'rest' of my time in Graz.
Finally, I want to thank my girlfriend Gabi Pfaffenbichler for supporting me with her kind and loving nature especially during the last year.

1. Introduction

According to the recent European Cardiovascular Disease Statistics from M. Nichols (2012) cardiovascular diseases are responsible for 40% of the deaths in the EU. Among these diseases, aortic aneurysms stand out because of their high mortality rate in cases of rupture ($85 - 95\%$ for abdominal aortic aneurysms (AAA) according to Kniemeyer et al. (2000)). Aortic aneurysms are permanent dilations of the vessel with a diameter 50% larger then in the healthy case, or for AAA specifically, a diameter larger then 3 cm (Shimizu et al. 2006). Most aneurysms tend to grow until rupture (Humphrey and Holzapfel 2012) and therefore must be treated in sight of the fatal consequences. Unfortunately the surgery itself carries a high risk and does not necessarily increase the survival rate (Lederle et al. 2002).

The development and growth of an aortic aneurysm goes hand in hand with structural changes within the vessel wall: collagen content is increased, elastin content is greatly reduced and smooth muscle cells degenerate (Tsamis et al. 2013). With this study we want to quantify the damage occurring in the aneurysm vessel wall due to multi-cyclic loading in the supra-physiological loading range based on data gathered from uniaxial extension tests. Further we want to quantify changes on the passive mechanical response due to remodeling during aneurysm development and growth, for diseased thoracic and abdominal samples, by appropriate constitutive modeling and correlation of these modeled mechanical parameters with data gathered in a previous study by Weisbecker et al. (2012) for healthy aortic tissue. By using identical testing devices and testing procedures we hope to increase the comparability and the significance of our results and are able to provide a meaningful basement for future finite element (FE) analysis.

FE simulations are already in use for estimating the influence on the tissue and minimizing the risk of some medical applications e.g. arterial clamping in Famaey et al. (2012), balloon-angioplasty in Balzani et al. (2006) or stent interaction in Mortier et al. (2010). An attempt to use FE analysis to estimate the rupture risk was performed, for example by Vande Geest et al. (2008), but only by calculating the maximum stress in the wall without any consideration of damage mechanisms.

In the present study we perform uniaxial extension tests on circumferentially and axially oriented strips from abdominal and thoracic specimens. The procedures are described in more detail in a previous work by Weisbecker et al. (2012), where corresponding tests on the healthy aortic wall were performed. We choose the uniaxial test, although biaxial testing would better mimic the physiological loading condition, because it is better suited to high loads and also smaller specimens can be tested. According to Holzapfel (2006) the disadvantages can be compensated for with a careful experimental protocol and constitutive model fitting procedure. By performing three loading cycles at different load steps we are

able to investigate both continuous and discontinuous softening.
The healthy arterial wall can be modeled as a fiber-reinforced composite with an isotropic matrix material, or from a biological viewpoint as an elastin matrix with reinforcing collagen fibers which are well-aligned and symmetrically oriented (Holzapfel et al. 2000). To take dispersion of the fibers into account this model was extended by Gasser et al. (2006). We use this extended formulation to model the mechanical response from the tissue after preconditioning. We assume that this model is also valid for diseased, which also means remodeled, tissue.

1.1. Mechanical tissue properties

Little experimental data for the stress-strain response of aneurysms exist. Biaxial tests performed by Vande Geest et al. (2006) on AAA samples showed a clearly non-linear anisotropic response, with a stiffer circumferential direction. Similar properties were reported by Tong et al. (2011) for AAA wall tissue covered by an intralumunal thrombus (ILT). Uniaxial extension testing of the separated layers of ascending thoracic aortic aneurysms (TAA) up to tissue failure was performed by Sokolis et al. (2012), also proposing a stiffer circumferential direction, but no cyclic loading was applied.
Most AAA walls are covered with an ILT, which itself is a three dimensional fibrin structure, with distinct biomechanical properties. Therefore it is necessary to consider its presence for accurate modeling of aneurysms. The three individual layers (luminal, medial and abluminal) were biaxially tested by Tong et al. (2011) and the luminal layer showed an age dependent direction dependency, starting from isotropic in early stages and turning anisotropic with age, in contrast the medial and abluminal layers remain isotropic. This age dependency is caused by structural changes within the thrombus, from an initially sponge-like material with fluid inside to a much stiffer fibrin network during time. This change of stiffness influences the underlying wall in terms of stress shielding and therefore the thrombus age should be considered as a critical risk factor for aneurysm rupture. In a subsequent work Tong et al. (2014) quantified structural remodeling and the influence on the strength of the structure by determine the change of dissection energy with time, considering four stages of development. The results show that for peeling through the thickness and within the separated layers the energy necessary to cause dissection decreases in the final stage after it was slightly increased during earlier stages of the remodeling process in some layers. This behavior represents the remodeling of the fibrin network, changing form thin to thick bundles followed by disruption of the network in the final stage of the thrombus.
Another structural element in vessel walls, with a great impact on the mechanical behavior, are plaques, containing lipids, fibro-fatty composites and calcifications. The presence of plaques carries additional risk for the treatment of aneurysm, especially in the case of rupture and subsequent stenosis. Depending on their consistence plaques influence the mechanical response and the geometry of the tissue. Commonly calcifications are divided in intimal or atherosclerotic, where the intimal layer thickens and hardens, and medial, which appear along the elastic lamina and stiffens the artery (Wu et al. 2013). To capture

the compressive response of plaque components Chai et al. (2013) performed indentation tests on 8 samples with low calcium content and calculated the compressive Young's modulus with an inverse FE algorithm. These results show a large variation in the stiffness within one plaque. Also different plaque types show significant variation of the mechanical response depending on the calcification to lipid ration (Mulvihill et al. 2013). This study suggests a clear distinction between stiffer plaques, containing more calcifications and softer liquid plaques not only in the stiffness of the material but also concerning failure properties. Softer plaques tend to rupture at comparable low stresses but on the other hand can withstand a higher amount of stretch until failure. By structurally analyzing the plaque tissue they identified voids within the tissue caused by calcifications which increased the vulnerability of the whole structure i.e. calcifications do not stabilize the tissue.

1.2. Rupture potential estimation of arterial tissue

There are many different approaches to estimate the rupture risk of aneurysms. A very fundamental one is the diameter criterion, which recommends surgery of aneurysms with a diameter larger then 5 - 5.5 cm and still despite its rudimentary nature this criterion has its big advantages. It can be measured with standard devices, such as ultrasound, and the result is available immediately. Another often used criterion, additionally to the maximum diameter, is the the growth rate, where the yearly growth is taken as a trigger for medical treatment. To achieve valid results the aneurysm has to be detected in an early state and it is not capable to make urgent decisions. At first view the diameter and the growth rate seem to be easily measured but through variable planes and elliptical cross-sections there is a lot of room for variations in the result. To overcome this disadvantages Kitagawa et al. (2013) suggest to measure the volume of the aneurysm what delivers, due to precise three dimensional imaging methods, first of all the CT scan, and modern image segmenting software tools, fast and accurate results. This images could open the way for calculating more sophisticated rupture risk estimations such as peak wall stress simulations. Improved methods are needed because many 'one criteria for all'approaches carry a possible fatal risk for an individual patient. Therefore future methods should tend toward patient-specific risk estimations, with a focus on finite element analysis (FEA). For a more detailed overview of rupture risk estimations the reader is referred to Vorp (2007) and Humphrey and Holzapfel (2012) or the recent work from Raut et al. (2013), where the influence of geometric and biomechanical factors on risk estimations are described. Subsequently some recent applications using analytic methods or FEA, with a focus on different assumptions for the boundary conditions and the material properties, are described.
An attempt to calculate the dissection risk using FEA was performed by Badel et al. (2014) for a coronary artery during the early stages of balloon angioplasty. In their simulation they considered the presence of a fibrous plaque and the embedding connective tissue, here the myocardium and the epicardium. Cohesive interfaces between the plaque and the media and within the media were added to simulate damage initiation and evolution. In accordance with clinical findings, these simulation showed a high risk of plaque detachment at

the shoulder region of the plaque. Additionally they propose a second risk zone within the arterial media where damage was initiated at a very early stage of the procedure. Also the damage initiation is very sensitive to the geometric configuration of the plaque and the surrounding tissue.
The influence of the lumen geometry, plaque morphology and composition on damage initiation and lumen gain due to overstretching during balloon angioplasty is simulated by Iannaccone et al. (2014). Therefore an anisotropic hyperelastic constitutive model to simulate the wall mechanics and a damage model for discontinuous, introduced by Balzani et al. (2006), is used. Their study showed eccentricity of the plaque causes high stresses in uncovered areas, which could lead to an increased failure rate during the procedure. According to their simulation soft plaques tend to fragmentation during the inflation process due to significant higher stresses within the fibrous cap compared to hard (calcified) plaques, while these stiffer plaques reduced the stress in the underlying tissue i.e. the underlying vessel wall is stress shielded.
Martin et al. (2013) tried to estimate the rupture potential of ascending thoracic aneurysms by calculating a failure diameter i.e. the diameter when the tension within the wall was higher then the ultimate tension gathered from uniaxial extension tests by using the law of Laplace in combination with data from uniaxial and biaxial tested specimens. Although they assumed the aneurysm wall to be a thin walled tube, they got results close to the clinically observed rupture diameters. Further they showed that an decreased compliance of the aneurysm wall is a mayor risk factor for rupture.
Regions with the highest rupture risk were determined by calculating the stress distribution and the thickness evolution of the vessel wall during inflation tests on ascending TAA tissue by Romo et al. (2014). By assuming that the wall behaves like a membrane and capturing the trajectories of the deformation no material parameters were needed to determine the stress distribution. Contrary to the general accepted theory that the tissue ruptures at the location of the highest stress they claimed the location where the thickness reduces the most is more prone to fail.
An approach for estimating the damage evolution and failure risk in growing aneurysms was developed by Volokh and Vorp (2008) and applied by Balakhovsky et al. (2014) (see references inside for more details). They extended an established growth and remodeling model with a failure criterion, in terms of an energy limiter constant, that provides a saturation value for the strain energy in the remodeling fibers. Therefore they modeled aneurysm as a membrane composed of collagen layers and the failure of single layers is considered to be responsible for the failure of the whole tissue. They calculated the rupture potential of two basic geometries, one should represent saccular aneurysms and the other fusiform aneurysms, with different initial fiber properties. Unfortunately they haven't validated their estimations with mechanical properties and geometries gathered from human aneurysmal tissues.

1.3. Damage models for soft biological tissues

There are different approaches to model damage that occurs in tissues, whereby continuum damage mechanics is well-established and elegantly simple. A scalar damage variable modifies the strain-energy function to handle difference in the loading and unloading parts of the stress strain response.

To describe softening in soft biological tissues continuous and discontinuous damage models were developed. In the continuous damage theory softening accumulates through the whole strain history and in contrast discontinuous damage is only accumulated when loads, that induce a strain energy higher then the previous maximum of the loading history, are applied.

A model that takes both softening effects into account was developed by Peña et al. (2009), where also different damage evolutions for the matrix and the different fiber families were considered. The model is able to fit preconditioning behavior and the Mullins's type softening very accurate but at the price of an complex experimental plan to gain all the parameters needed.

Balzani et al. (2006) introduced a model for discontinuous damage and calibrated it successfully in an subsequent work (Balzani et al. 2012) with one experimental data set from a human carotid artery. The author assumed that damage only accumulates in the collagen fibers, an assumption which was validated by Weisbecker et al. (2012).

Another approach was taken by Rodríguez et al. (2006), where collagen fibers were modeled as worm-like chains, and where the discontinuous softening was realized by different strain energies until fracture for each collagen fiber bundle. This was achieved by considering the rupture strain as a Beta distributed variable. Subsequently, this approach was implemented in an FE code by Rodríguez et al. (2008) to estimate the rupture risk of AAA tissue.

Gasser (2011) developed a microfiber model to describe the failure of collagen fibers due to irreversible rearrangements when supra-physiological loading is applied. The loss of proteoglycane bridges that causes softening of the tissue is quantified by a single damage parameter. This approach can be understood as an multi-scale model where the overall tissue properties are derived by integrating the properties of the spatial distributed collagen fibers over the unit sphere. This model takes advantage of the fact that at the molecular level the cross linking of collagen fibrils is very well understood. To apply this model, material parameters are estimated from the macroscopic mechanical test data, because the macroscopic data is supposed to mimic the in-vivo condition more accurate then microscopic properties of single collagen molecules. The model is able to capture the low and high strain region of the stress strain response and also preconditioning of the tissue.

The first attempt to model the softening behavior including all occurring inelastic effects i.e. hysteresis of the mechanical response, stress relaxation, residual strain and creeping of the residual strain comes from Rickaby and Scott (2013). They employed a transversely isotropic eight-chain model and modified it by adding softening functions for the primary loading path, the unloading and reloading path. Additionally separate functions for the

creep behavior and the stress relaxation were considered. They have fitted a longitudinal and circumferential data set from a tested human thoracic aorta and got an excellent accordance but it seems impossible to interpret the physiological meaning of the numerous parameters.
In the present work we use a pseudo-elastic constitutive model, introduced by Ogden and Roxburgh (1999), to quantify the damage that accumulates in the aortic tissue and causes softening. A big advantage is that the fitting procedure for the model can be split into two parts. First the primary loading curve, which is described by an elastic strain-energy function, is fitted and then the unloading and reloading curves of this function are used to fit the variables. In this study we do not set a threshold value for the damage, in opposite to other authors like Balzani et al. (2006), who took the strain-energy accumulated at internal pressure of 180 mmHg as the initial damage state and prohibited the evolution of softening below this level. Because to little is still known about the damage mechanisms within the tissue and the tolerance level towards tension. There must be distinguished if softening is still in the physiological range, like in the case of preconditioning and when it starts to cause irreversible, fatal damage to the structure.
In the following sections the constitutive model is presented and the experimental protocol and data analysis methods are explained. The material and damage parameters obtained and the results from the histological investigations are presented and subsequently, with regard to some limitations of this study, discussed.

2. Methods

2.1. Constitutive Modeling

2.1.1. Pseudo-elastic damage model

To model the material response of AAA tissue and to facilitate comparison between healthy and diseased tissue we use the procedure described in Weisbecker et al. (2012). Thereby we use a decomposed pseudo-elastic damage model defined as (Ogden and Roxburgh 1999)

$$\Psi(J, \overline{\mathbf{C}}, \eta) = \Psi_{\text{vol}}(J) + \eta\overline{\Psi}^{0}(\overline{\mathbf{C}}) + \Phi(\eta), \tag{2.1}$$

where Ψ_{vol} describes the volumetric elastic response, $\overline{\Psi}^{0}$ denotes the isochoric strain energy of the undamaged material, which describes the isochoric elastic response (the superscript 0 denotes an undamaged material), $\Phi(\eta)$ in (2.1) denotes a (smooth) damage function, $\overline{\mathbf{C}}$ denotes the modified Cauchy-Green tensor according to Holzapfel et al. (2000) and J is the determinant of the deformation gradient. Note that damage is only accumulated in the deviatoric part of the strain-energy function and that the material remains isochoric even if damage is induced. Here η is the damage variable and according to Weisbecker et al. (2012) defined as

$$\eta = 1 - \frac{1}{r}\text{erf}\left[\frac{1}{m}(\overline{\Psi}^{\max} - \overline{\Psi}^{0})\right], \tag{2.2}$$

where $r > 1$ characterizes the maximum material damage that can be induced under loading, and $m > 0$ determines how fast softening is accumulated. Small values of m indicate that significant damage occurs already at small strains, whereas for larger values of m damage will progress more slowly. $\overline{\Psi}^{\max}$ denotes the maximum strain-energy obtained in the deformation history. We characterize induced damage by the minimum of the damage variable as

$$\eta^{\min} = 1 - \frac{1}{r}\text{erf}\left(\frac{1}{m}\overline{\Psi}^{\max}\right). \tag{2.3}$$

With (2.1) the second Piola-Kirchhoff stress tensor can be calculated as $\mathbf{S} = 2\partial\Psi/\partial\mathbf{C} = \mathbf{S}_{vol} + \overline{\mathbf{S}}$, with $\mathbf{S}$ is given by $\mathbf{S}_{\text{vol}} = 2\partial\Psi_{\text{vol}}(J)/\partial\mathbf{C}$ and $\overline{\mathbf{S}} = \eta\overline{\mathbf{S}}^{0}$ where $\overline{\mathbf{S}}^{0}$ is the isochoric second Piola-Kirchhoff stress tensor according to the primary loading curve.

2.1.2. Constitutive model for arterial tissue

The arterial wall is modeled as a fiber reinforced composite with two fiber families, as introduced in Gasser et al. (2006) and experimentally shown in, e.g., Finlay et al. (1995)

for human brain arteries and Schriefl et al. (2011) for human abdominal aorta. The strain-energy function $\overline{\Psi}^0$ can be decomposed as

$$\overline{\Psi}^0 = \overline{\Psi}^0_{\mathrm{m}} + \overline{\Psi}^0_{\mathrm{f}}, \tag{2.4}$$

where $\overline{\Psi}^0_{\mathrm{m}}$ is the energy stored in the non-collagenous matrix, which is modeled as a neo-Hookean material with an initial shear modulus μ, and $\overline{\Psi}^0_{\mathrm{f}}$ an energy stored in the collagen fibers. The related anisotropic strain energy function for the collagen fibers can be written as

$$\overline{\Psi}^0_{\mathrm{f},i} = \frac{k_1}{2k_2}[e^{k_2(\bar{I}_i^\star-1)^2} - 1], \qquad \bar{I}_i^\star = \kappa\bar{I}_1 + (1-3\kappa)\bar{I}_i, \qquad i = 4, 6, \tag{2.5}$$

where $i = 4, 6$ is related to the two fiber orientations. The pseudo-invariant $\bar{I}_4 = \overline{\mathbf{C}} : \mathbf{M}\otimes\mathbf{M}$ and $\bar{I}_6 = \overline{\mathbf{C}} : \mathbf{M}' \otimes \mathbf{M}'$ corresponds to the square of the stretches of the fibers in the mean fiber direction. The fibers are oriented symmetrically with respect to the circumference of the arteries and the vectors $\mathbf{M}$ and $\mathbf{M}'$ denote the mean direction of the fibers in the reference configuration which can be described by a single angle φ, between the circumferential direction and the mean fiber direction. The dispersion parameter κ describes the radial symmetry of the dispersion about the fiber direction, k_1 is a stress-like parameter and k_2 is dimensionless. According to Weisbecker et al. (2012) we assume that the damage is only related to the collagen fibers. Hence $\overline{\mathbf{S}}$ can be described as

$$\overline{\mathbf{S}} = \overline{\mathbf{S}}_m + 2\eta_f\overline{\mathbf{S}}^0_f, \qquad \overline{\mathbf{S}}^0_m = 2\frac{\partial\overline{\Psi}_{\mathrm{m}}}{\partial\mathbf{C}}, \qquad \overline{\mathbf{S}}^0_f = 2\frac{\partial\overline{\Psi}^0_{\mathrm{f},i}}{\partial\mathbf{C}}. \tag{2.6}$$

With a standard push forward operation we obtain the Cauchy stress tensor $\sigma = J^{-1}\mathbf{F}\mathbf{S}\mathbf{F}^T$.

2.2. Experimental Protocol

2.2.1. Sample preparation

For this study samples from 12 abdominal (69.7 years $\pm$ 4.4, mean $\pm$ std) and 7 thoracic [1] (64.5 years $\pm$ 12.3 years) aortic aneurysms were harvested in Leuven (Belgium), stored in physiological solution and frozen. The collected specimens were all true fusiform aneurysms. After transportation to Technical University of Graz they where were stored in the freezer at $-20°$C. For the present study, the use of autopsy material from human subjects was approved by the Ethical Committee of Universitaire Ziekenhuizen Leuven, with the approval number B32220071899. After unfreezing the samples, loose connective tissue attached to the adventitia was carefully removed in preparation for mechanical testing, so that only the wall itself remained. The samples were stored in physiological solution

[1] unfortunately one data sheet from a sample got lost during the transport from the hospital in Leuven to the laboratory in Graz, so the given mean value is calculated from the remaining 6 sheets with patient specific data

between preparation and testing to prevent dehydration. Rectangular pieces were cut out in the axial and in the circumferential direction of the tissue with a punching tool. Samples measured a width of 4 mm and a length of at least 15 mm.

Overall we were able to test abdominal tissue from eight donors (denoted as A.1 - A.8) and thoracic tissue from six donors (T.1 - T.6). To increase the amount of mechanical data we took more then one sample pair per donor, if the size of the tissue specimen was big enough (further on denoted with an additional index, e.g. A.8.1)

Sample thickness was measured with a videoextensiometer (ME 46-350, Messphysik, Fürstenfeld, Austria) at four different points distributed evenly on the sample. To get a representative thickness for the sample the mean value of the four measurements was calculated. The videoextensiometer was calibrated before every thickness measurement and before the mechanical testing.

Table A.1 shows data concerning the medical background and lifestyle of the patients. Only five out of six donors with thoracic aortic aneurysms are listed because for one donor no data was available. It should be mentioned that nearly all patients had hypertension and hypercholesteroma, both known risk factors for cardiovascular diseases. A table with additional data providing some information of the medical background and the lifestyle of the donors is provided in A. Close to the tested areas samples were cut out and stored in a 4% buffered formaldehyde solution (pH 7.4) for histological investigations.

Donor	Gender	Age	Length	Weight	BMI	Diameter
-	-	y	cm	kg	-	mm
Thoracic aorta						
T.1	f	75	158	45	18.02	46
T.2	f	78	167	70	25.09	58
T.3	f	73	156	53	21.77	-
T.4	m	51	173	83	27.73	48
T.5	m	51	186	98	28.32	49
Abdominal aorta						
A.1	m	73	175	85	27.75	73
A.2	m	59	178	73	23.04	59
A.3	m	60	162	83	31.62	60
A.4	m	70	176	88	28.40	70
A.5	f	60	169	75	26.20	60
A.6	f	52	165	87	31.95	52
A.7	m	52	174	75	24.77	52
A.8	m	85	166	70	25.40	85

Table 2.1.: Patient specific data for the specimens tested.

2.2.2. Uniaxial tension test

We performed mechanical testing of axial and circumferential strips in a bath of physiological solution, kept at a constant temperature of 37 °C, with uniaxial testing machine (μ -Strain ME 30-1, Messphysik, Fürstenfeld, Austria). Sandpaper was glued at the small ends of the sample to guarantee a tight connection to the testing device in the clamps. Small rectangular markers were attached to measure the displacement during the testing procedure with the videoextensiometer (ME 46-350, Messphysik, Fürstenfeld, Austria). The markers were made of foam material to minimize reflections that could cause problems with the length measurement. The testing procedure was force driven. Forces were calculated so that the loading leads to the desired first Piola-Kirchhoff stresses of $25, 50, 75, 100, 200, 300$ kPa. For every load step three loading cycles were performed to observe discontinuous softening in the first loading cycle and further continuous softening in the two following cycles at the same load. The testing was performed under quasi-static conditions with a load rate of 5 mm/min, to avoid dynamic or viscoelastic effects.

2.2.3. Data analysis

Data analysis was done using a semi-automatic fitting procedure in Matlab (R2011b, The MathWorks, Inc., Massachusetts, United States). Force and displacement data sets were preprocessed to eliminate data which were recorded after rupture of the sample or when the sample slipped out of the clamps.
To fit the constitutive damage model to the data, first the stretch $\lambda = l/L$ was calculated, where l is the deformed length of the sample and L is the reference length, according to the undeformed sample, in the loading direction. Subsequently the Cauchy stress was calculated as

$$\sigma = \frac{f}{TW}\lambda. \tag{2.7}$$

where T is the initial thickness and W the initial width of the material, cf. Weisbecker et al. (2012).
We also assume that the damage evolves equally in both fiber families so that the damage can be fully described by the two parameters r and m.
To reduce noise, the measured stress and stretch were filtered with a Savitzky-Golay Filter of order 2. The frame size of the filter varied from specimen to specimen (from min. 41 data points to max. 151 data points), depending on the noise, but kept as low as possible to achieve a good fit without manipulating the data. Fitting was done by using the nonlinear least square trust region algorithm implemented in Matlab. As a first step, the material parameters $\mathbf{x}_m = [\mu, k_1, k_2, \varphi, \kappa]$ were fit to the primary loading curve. Therefore stretch lateral to the loading direction was calculated using the constraint that the stress in this direction has to equal 0. Subsequently, due to the incompressability condition $\lambda_1\lambda_2\lambda_3 = 1$, where the indices $1, 2, 3$ denote three perpendicular directions, the stretch through the thickness was calculated. The calculated stretches and stresses where used to minimize the objective function

$$\chi = \sum_{i=1}^{n} [\sigma_i^{model}(\mathbf{x}_j) - \sigma_i^{exp}]^2, j \in [m, d], \tag{2.8}$$

where n denotes the number of data points, σ^{exp} the Cauchy stresses obtained experimentally and σ^{model} the Cauchy stresses calculated from the strain-energy function Ψ for the axial and the circumferential directions simultaneously and $\mathbf{x}$ denotes a vector of model parameters. The subscript j denotes which part of the parameters are fit, i.e., m denotes the material parameters and d the damage parameters. Once the material parameters are obtained the lateral and through the thickness stretches were updated at every iteration step until the solution converged. To improve the accuracy of the fit in the toe region of the loading curve, an initial fit was performed, where this toe region was fitted separately, to obtain the shear modulus μ that is largely responsible for the material behavior at low deformations. To obtain the damage parameters $\mathbf{x}_d = [r_f, m_f]$ the fitting procedure was repeated, by minimizing (2.8) using the fitted constitutive parameters and the entire loading history. The fitted material parameters are reported as median values with their corresponding interquartile ranges.

2.2.4. Statistical analysis

The correlation between the age, the BMI and the preoperative aneurysm diameter is calculated with the rank correlation coefficient r_s. The significance of the correlation is tested by calculating the confidence interval with the Fisher transformation. These correlations were only calculated for the abdominal specimens, because of insufficient patient data for the thoracic specimens. Significance of the differences between the mechanical data gathered from the abdominal and thoracic diseased specimens, and the differences between healthy (Weisbecker et al. 2012) and the diseased tissue, is investigated with the Wilcoxon rank sum test. The mechanical data from the diseased ascending thoracic tissue samples are compared to data from healthy descending thoracic tissue, although we know that there are differences in the mechanical properties between ascending and descending thoracic aortic tissues (Roccabianca et al. 2014), we assume that we can capture some trends in the changing mechanical behaviour due to aneurysm growth. The significance level was adjusted with the Boferroni-Holm correction. For all tests $p < 0.05$ was assumed to be significant.

2.2.5. Histology

A formalin fixed and parafin embedded cut in the circumferential plane, normal to the axial direction of the sample was investigated histologically. Samples were stained, following standard procedures, with Hematoxylin and Eosin (H& E) to highlight cell cores, Picrosirius Red (PSR) to highlight fibrillar collagen and Elastica von Gieson (EvG) to highlight elastic fibers. The staining was performed at the Institute of Pathology from the Landeskrankenhaus Graz.

3. Results

3.1. Material and damage parameter

Representative stress-stretch response for an abdominal specimen is shown in Fig. 3.1 (a) and for a thoracic specimen on in (c). Both specimens show an anisotropic behavior and a significant hysteresis. The material and damage parameters $\mu, k_1, k_2, \varphi, \kappa, r_f$ and m_f obtained, with the coefficient of determination R^2, the median and the first and third quartile, Q_1 and Q_3 are shown in Table 3.1. The mean thickness for the abdominal specimens was 2.12 ± 0.43 mm and 1.98 ± 0.3 mm for the thoracic ones (all the measured thicknesses are listed in B.1).

3.2. Data statistics

Only the BMI has a statistical relevant correlation with the material properties of AAA tissue, both k_1 and κ increase with increasing BMI. The rank correlation coefficient r_s for k_1 was 0.71 and the corresponding confidence interval $[0.09, 0.93]$, while for κ r_s was 0.78 with CI $[0.23, 0.95]$. The statistical analysis provided no correlation between the fitted material parameter for neither the diameter nor the age. Statistically relevant differences ($p < 0.05$) between diseased abdominal and thoracic specimens was found for k_1 and κ, both are higher in abdominal specimens.

3.3. Comparison with healthy tissue

Table 3.2 reviews the material parameters for healthy tissue from Weisbecker et al. (2012). Statistically significant differences for the abdominal specimens were found for the angle φ and the damage variable m_f. The obtained fiber angle for AAA tissue is close to $45°$. The damage variable, an indicator for the strain dependency, is smaller in the diseased case. The constitutive parameters μ and k_2 for the thoracic aneurysm tissue differ significantly from the corresponding healthy ones. The shear modulus is higher, indicating a higher initial stiffness, while the smaller k_2 corresponds to a reduced exponential stiffening.

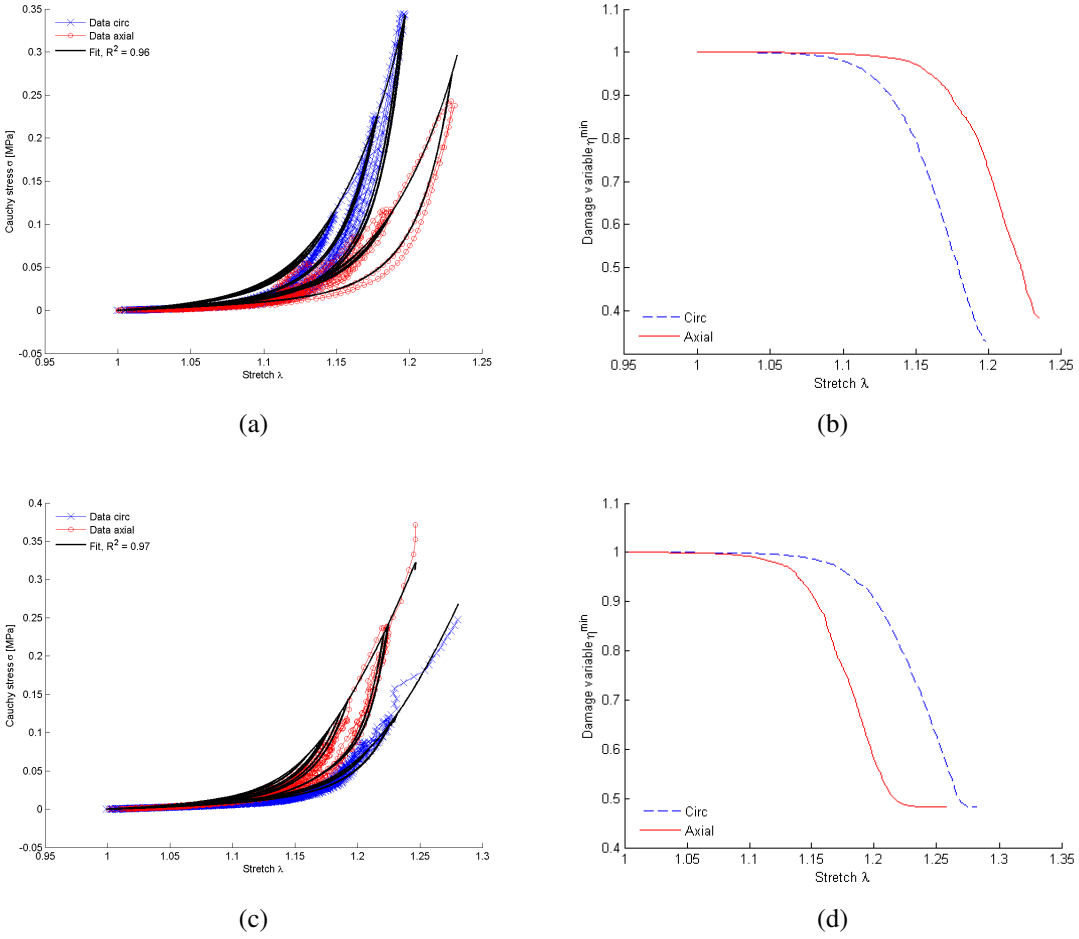

Figure 3.1.: Representative stress-stretch responses for abdominal sample A.8.2 (a) and thoracic sample T.2.1 (c). The corresponding evolution of the damage variable for the abdominal specimen is shown in (b) and for the thoracic specimen in (d). The corresponding histological images are provided in Figs. 3.3 and 3.2, respectively

Donor	μ MPa	k_1 MPa	k_2 -	φ °	κ -	r_f -	m_f -	R^2 -
Thoracic aorta								
T.1.1	0.046	7.92	0.000	50.7	0.145	1.00	0.026	0.94
T.1.2	0.023	5.38	0.000	48.6	0.134	1.00	0.033	0.97
T.2.1	0.018	1.92	0.000	46.6	0.135	1.93	0.002	0.97
T.2.2	0.035	9.07	0.000	34.6	0.256	1.00	0.007	0.97
T.3.1	0.028	0.57	94.626	41.8	0.000	2.03	0.002	0.97
T.3.2	0.019	0.68	0.005	41.4	0.018	2.69	0.003	0.97
T.4.1	0.020	0.24	4.998	43.6	0.039	2.22	0.006	0.97
T.4.2	0.016	0.19	4.943	44.8	0.037	3.03	0.005	0.97
T.5.1	0.026	0.48	3.470	46.3	0.000	3.07	0.003	0.98
T.5.2	0.025	0.15	4.930	45.7	0.052	3.39	0.004	0.99
T.6.1	0.035	0.12	2.500	41.4	0.000	2.11	0.004	0.96
Median	0.025	0.57	2.500	44.8	0.039	2.11	0.004	0.97
$[Q_1, Q_3]$	$[0.019, 0.033]$	$[0.20, 4.52]$	$[0.000, 4.939]$	$[41.5, 46.5]$	$[0.005, 0.135]$	$[1.23, 2.94]$	$[0.003, 0.007]$,	$[0.97, 0.98]$
Abdominal aorta								
A.1	0.010	6.16	0.001	41.4	0.249	2.10	0.002	0.92
A.2	0.008	1.54	67.176	41.5	0.104	1.00	0.008	0.96
A.3	0.034	15.09	569.230	41.4	0.270	3.10	0.002	0.90
A.4	0.034	16.52	0.000	43.1	0.266	3.08	0.004	0.95
A.5	0.173	54.52	30.369	48.2	0.316	1.50	0.001	0.92
A.6	0.080	6.03	0.000	39.1	0.252	1.26	0.003	0.87
A.7	0.012	2.08	0.000	41.9	0.151	1.50	0.004	0.94
A.8.1	0.019	2.72	0.000	43.9	0.174	1.20	0.005	0.94
A.8.2	0.026	2.74	119.568	43.2	0.181	1.35	0.004	0.96
Median	0.026	6.03	0.001	41.9	0.249	1.50	0.004	0.93
$[Q_1, Q_3]$	$[0.011, 0.046]$	$[2.56, 15.45]$	$[0.000, 80.274]$	$[41.4, 43.4]$	$[0.169, 0.267]$	$[1.21, 2.34]$	$[0.002, 0.004]$	$[0.91, 0.95]$

Table 3.1.: Constitutive parameters for the diseased wall of the human thoracic and abdominal aortas; together with the coefficient of determination R^2, the median, the first quartile Q_1 and the third quartile Q_3.

	μ MPa	k_1 MPa	k_2 -	φ °	κ -	r_f -	m_f -	R^2 -
Thoracic aorta								
Median	0.017	0.56	16.21	51.0	0.18	1.59	0.008	0.97
$[Q_1, Q_3]$	$[0.014, 0.019]$	$[0.24, 0.94]$	$[5.79, 34.79]$	$[46.8, 53.8]$	$[0.08, 0.28]$	$[1.25, 1.83]$	$[0.004, 0.011]$	$[0.95, 0.98]$
Abdominal aorta								
Median	0.019	5.15	8.64	38.8	0.24	1.10	0.013	0.98
$[Q_1, Q_3]$	$[0.012, 0.042]$	$[2.58, 10.52]$	$[0.00, 32.40]$	$[35.8, 41.1]$	$[0.21, 0.25]$	$[1.00, 1.54]$	$[0.010, 0.019]$	$[0.93, 0.99]$

Table 3.2.: Median values and interquartilar range for constitutive parameters for the intact (three-layer composite) wall of the human thoracic and abdominal aortas from Weisbecker et al. (2012).

3.4. Histology

Representative histological cuts are shown for a AAA specimen in Fig. 3.3 and for a TAA specimen in Fig. 3.2. The first row of each figure shows the H&E staining, where cell cores are stained dark purple. The mid row shows the EvG staining where the elastic fibers are highlighted black. The bottom row shows the PsR staining, with collagenous fibers stained red. The pictures were acquired with a Nikon Digital Sight DS-Fi 1 , on the left hand side the magnification of the microscope (Nikon Eclipse 80i) was set to 20x and on the right hand side to 100x. From top to bottom figures always show the same section of the specimen.

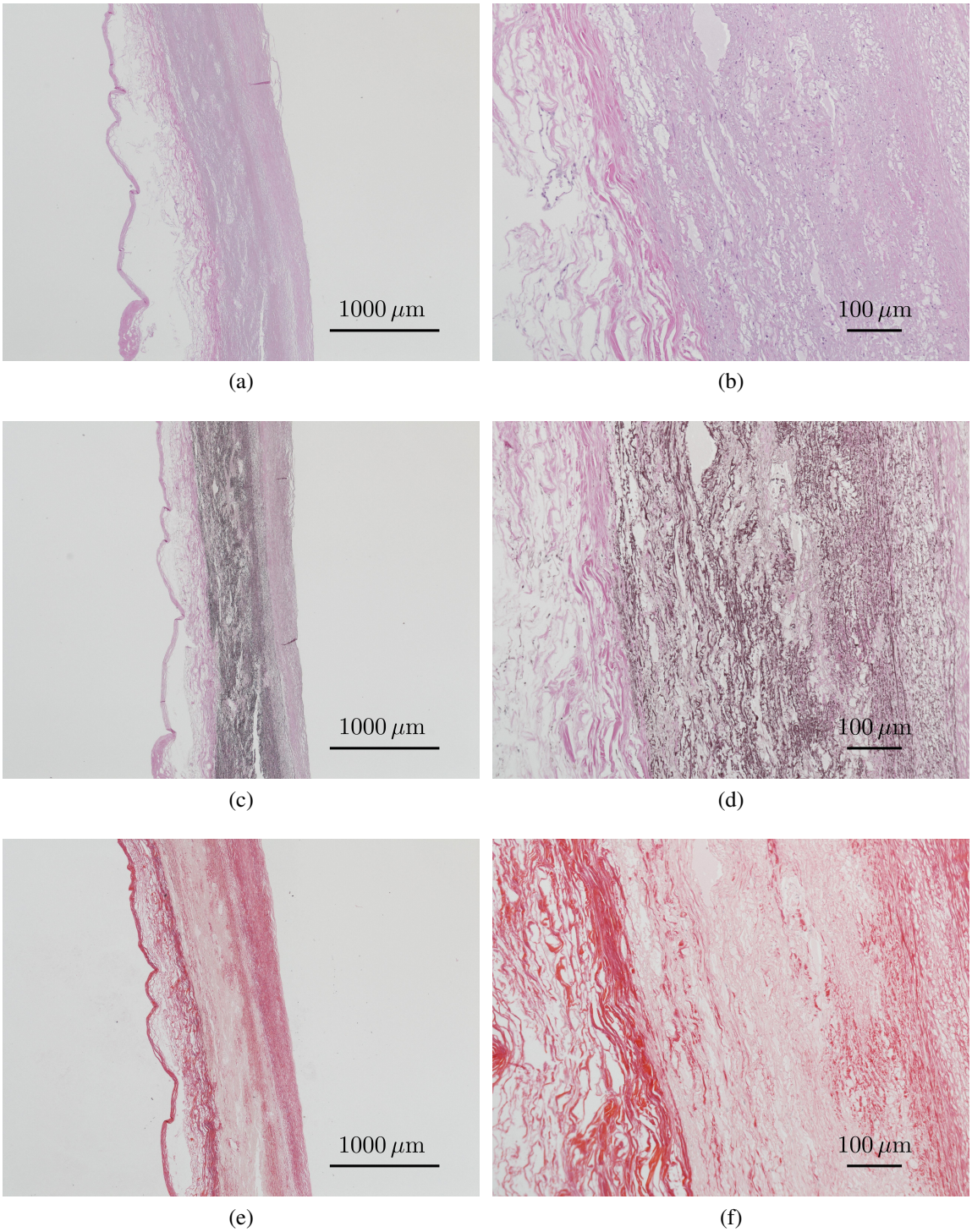

(a) (b) (c) (d) (e) (f)

Figure 3.2.: Representative histological cuts from thoracic specimen T.2. HE staining (top), EvG staining (middle) PsR (bottom) from the whole wall on the left side and a magnified segment on the left side. The corresponding mechanical test data and model fit are provided in in Figs. 3.1c and 3.1d. The scale bar on the left hand side is 1000 μm and on the right hand side 100 μm

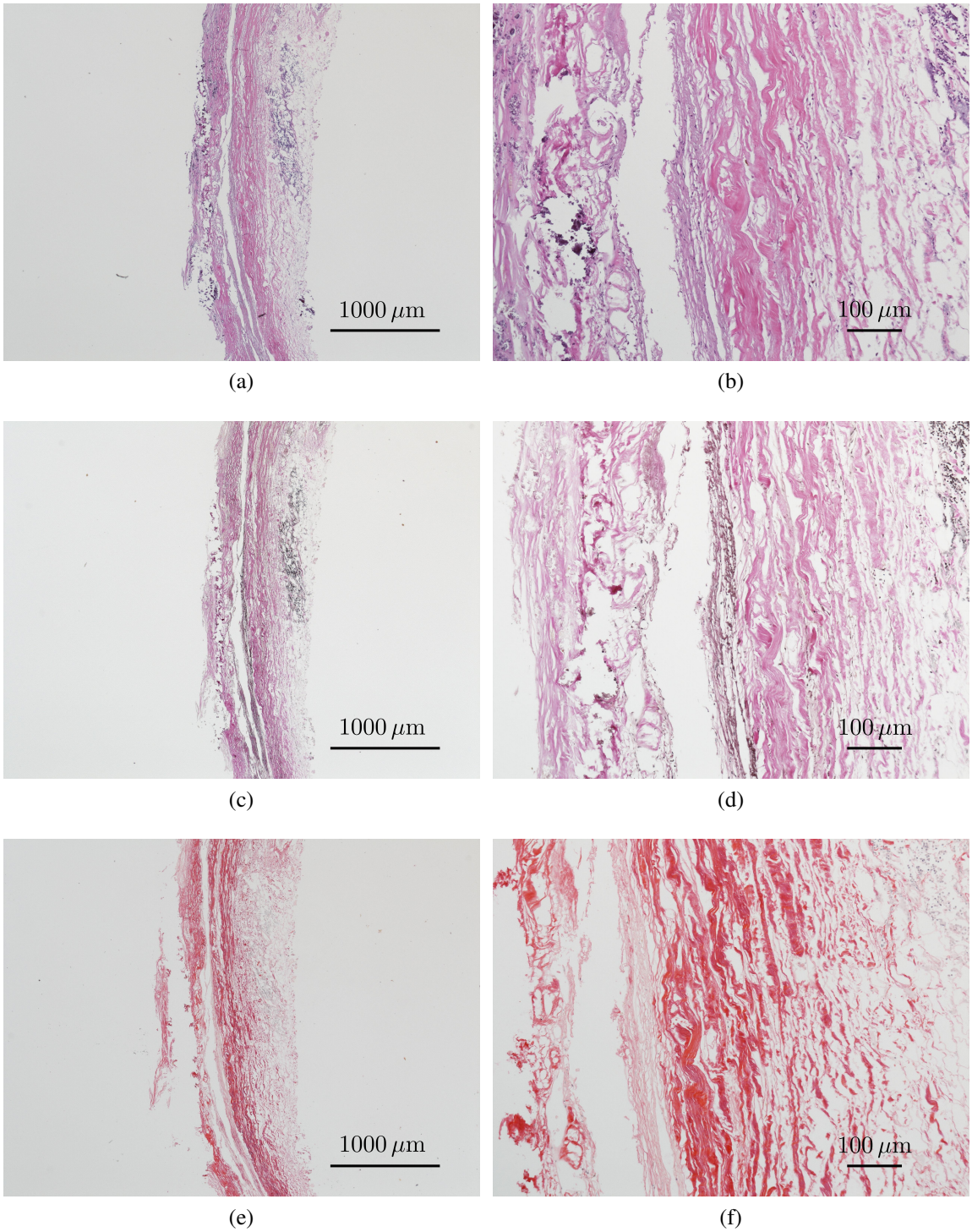

Figure 3.3.: Representative histological cuts from abdominal specimen A.8. HE staining (top), EvG staining (middle) PsR (bottom) from the whole wall on the left side and a magnified segment on the left side. The corresponding mechanical test data and model fit are provided in in Figs. 3.1a and 3.1b. The scale bar on the left hand side is 1000 μm and on the right hand side 100 μm

4. Discussion

The main goal of this study was to obtain material parameters for abdominal and thoracic aortic aneurysmal tissues to facilitate FE Analysis and to find out more about significant differences or similarities between AAA and TAA tissue as well healthy versus aneurysmal tissue. Therefore the stress stretch response of the material was modeled with an anisotropic pseudo-elastic damage model previously fitted to healthy aortic tissues in Weisbecker et al. (2012). Correlations between the location and patient-specific properties with the mechanical data were checked and the obtained material parameters are compared to a previous study with healthy tissue by Weisbecker et al. (2012). To gather additional information about the structure and the distribution of the load bearing components we investigated histological cuts.

4.1. Material and damage parameter

The representative plots in Fig. 3.1(a) and Fig. 3.1(c) show the the data gathered from mechanical testing and the fitted stress stretch response. In both cases the model fits the data well. On one side the primary loading curve but also the discontinuous softening caused by pre-conditioning in the physiological loading range and actual damage in the supra-physiological loading range. We were not able to define a threshold to distinguish between physiological and non-physiological damage and therefore more specialized experiments and structural analysis have to be performed, which is challenging as long as the damage mechanisms, which ultimately lead to failure, are not well understood (Gasser 2011). The corresponding evolution of the softening, represented by the minimum of the damage variable, is shown on the right hand side in Fig. 3.1(b) and Fig. 3.1(d). Compared to healthy tissue from Weisbecker et al. (2012) the evolution of the softening initiates at smaller strains. The material response is clearly anisotropic for both cases but the orientation switches. In the abdominal case the circumferential direction is stiffer and in this thoracic case the axial direction is stiffer.
The fitted parameters are not normally distributed, therefore we took the median value and the corresponding interquartile range to represent them correctly, with the additional benefit that these values are not as sensitive to outliers as the mean value and standard deviation.
The median fiber angle φ for the thoracic samples is $44.8°$, indicating a nearly isotropic behavior, but its interquartile range from $41.5°$ to $46.5°$ shows the high variability of the mean fiber orientation from a circumferentially to an axially reinforced composite. These findings are in contrast to Sokolis et al. (2012) where all separated layers were determined

stiffer in the circumferential direction and in Pham et al. (2013) where they also got a stiffer circumferential direction for the intact wall under biaxial loading. But on the other side Azadani et al. (2013) proposed that there is no directional dependency for TAA tissue, which is in accordance to the median value we found. This variation indicates that taking the median value could have a large impact on the reliability of, e.g. stress calculations with FEA. With improving imaging techniques, such as e.g. optical coherence tomography (van Soest et al. 2010), intravascular ultrasound (Suzuki et al. 2008) or B-mode ultrasound (de Groot et al. 2008), in vivo estimation of the tissue state might allow an accurate implementation of location dependent material properties and therefore the range of material parameter might be of higher interest then median values, a simplified attempt in this direction was already performed by Kaladji et al. (2013) with an varying Young's modulus depending on the imaged based estimated calcification level of a human arterial wall along the path of the guidewire during a simulated stent insertion for endovascular aortic aneurysm repair. In contrast the AAA specimens with a median value of $\varphi = 41.9°$, with an interquartile range from $41.4°$ to $43.4°$, show a primarily circumferential fiber orientation and subsequent a higher stiffness in this direction, with less variation. Similar results are proposed in Tong et al. (2011) and Vande Geest et al. (2006). It would be of great interest, on one side to validate the proposed mean fiber angles but also to improve the accuracy of the fit for the stiffness related parameters (Rodríguez et al. 2009), to additionally measure the fiber direction and the dispersion with the approach developed by Schriefl et al. (2013), where the tissue is optically cleared and fiber angles are measured using second harmonic generation based imaging.
The k_2 values for the AAA tissue vary widely between zero, meaning no exponential but quadratic stiffening (the strain-energy function from (2.5) is reduced to $\overline{\Psi}^0_{\mathrm{f},i} = k_1(\bar{I}^\star_i - 1)^2/2$), and relatively high values. This shows the high heterogeneity of the tissue, with very stiff, highly calcified areas and much softer regions. Here again, naive use of the median value could also lead to serious errors in simulations. Although some limited applications in biomechanics exist, where the stress distribution can be calculated without material parameters e.g. for intracranial aneurysms, which can be appropriately assumed as thin walled tubes and therefore the stress distribution can be obtained by inverse analysis, the determination and correct use of appropriate material parameters for approaches, where the tissue properties are an inescapable component of the problem, like in the case of AAA's and TAA's, remains a major challenge in biomechanics (Miller and Lu 2013).

4.2. Statistics

A significant difference between the AAA and the TAA tissue was found for the parameter k_1 which is higher for the abdominal tissue, indicating a higher stiffness in the low stretch region. Also κ differs significantly, indicating a much higher fiber dispersion in the abdominal specimens, but because we must take into account that the collagen fibers are a non-symmetrical distributed and therefore the κ parameter doesn't mimic the actual configuration in an optimal way (Schriefl et al. 2011).

When correlated to patient data, it is interesting that the diameter has no significant influence on the mechanical properties, which is in accordance with results across the literature e.g. Vorp (2007), and strengthens the theory that the diameter is an inappropriate measurement to trigger surgery. Also no correlations are evident for the patient age, indicating that the age of the aneurysm itself is more important on its mechanical properties, witch is consistent with the findings of Wilson et al. (2012). But the small sample population could also cause the lack of significant correlations.
A significant difference in the fiber angle φ was found between healthy and diseased abdominal tissue. The fibers are also aligned circumferentially but they are closer to an isotropic distribution with an angle $\varphi = 45°$, which is in contrast to Vande Geest et al. (2006) where an increased anisotropy due to aneurysm development is proposed. The damage parameter m_f is significantly lower for AAA tissue then in healthy tissue indicating that significant softening is already induced at smaller strains. For a correct interpretation of these results it is inevitable to consider the condition of the tissue, if significant calcifications are evident it is most likely that here the softening can be interpreted as non physiological i.e. damage (Mulvihill et al. 2013).
For the thoracic specimens the parameters μ and k_2 vary significantly between healthy and diseased tissue, μ is higher, indicating a higher stiffness in the low strain region, which can be due to remodeling of the elastic ground substance to a collagenous network, with increased cross-linking of the collagen fibers, according to Lindeman et al. (2010). The same group also showed that the collagen fibrils have a reduced waviness and thereby appear stiffer at lower stretches. This is consistent with our findings that the parameter k_2 is lower which means a reduced exponential stiffening of the material occurs compared to the healthy tissue, which could be due to a faster fiber recruitment at lower strains in the remodeled collagen network.

4.3. Comparison with healthy tissue

The diseased AAA tissue shows similar behavior compared to the healthy one, the median values for μ and k_1 are slightly higher, indicating higher initial stiffness. The median value k_2 is close to zero, so the material has a response which is quadratic rather than exponential in behavior, but in general the variation of the mechanical properties is higher in the diseased tissue, which could be related to the fact that in the study of Weisbecker et al. (2012) samples with signs of atherosclerosis, which leads to less heterogeneous samples, were avoided in contrast to this study.
It seems in general that aneurysm development has more effect on the mechanical properties of a thoracic aorta then on an abdominal aorta. Some remodeling processes, e.g. the decrease in elastin, the increase in collagen and also atherosclerosis happen in the aorta without disease as a normal process due to aging, as reported in Tsamis et al. (2013). These effects might be more distinct in the abdominal aorta and so the tissue in its initial condition, which has an important effect on the development of the disease (Wilson et al. 2012), is already more remodeled and so the changes due to the disease are not as influential as

for the thoracic tissue.
The median values for the damage variable r_f are higher for the diseased tissues then for the healthy tissues. Therefore less softening can occur in the diseased tissue, which indicates that the remodeling process weakens the tissue, but again more research hast to be conducted to identify damage beyond the tissues tolerance level, because, as presumed for restenosis occurring after stent implantation, damage is most likely a trigger for remodeling processes (Timmins et al. 2011) and could also be responsible for stabilized aneurysms with a vanishing failure risk as reported in Vorp (2007). Notice that the difference in r_f between abdominal and thoracic tissue remains nearly constant for the healthy and diseased tissue, which again emphasizes the importance of the initial condition of the tissue on the development of aneurysms.

4.4. Histology

The main goal of the histological investigation was to get an overview of structural changes within the wall due to the aneurysm, and to compare them to data from the mechanical testing to get a rough validation on the reasonableness of the obtained material parameters. The histological study showed a significant difference between the TAA and the AAA specimens. The arterial wall of the AAA specimens was highly remodeled in terms of the connective tissue, the number of elastic fibers and smooth muscle cells was drastically reduced and replaced by collagen fiber bundles. This is shown in the representative histological pictures in Fig. 3.3: in Fig. 3.3(c) the absence of smooth muscle cells is visible, the overview Fig. 3.3(e) shows the absence of elastin over wide areas of the sample, which is replaced by collagen as show in Fig. 3.3(d). Due to the degeneration of the active cell components, the mechanical properties of a highly remodeled AAA might be obtained in a realistic way with passive testing alone. Also signs of atherosclerosis, in terms of high calcification, shown as crystalline structures in the histological cuts, for example on the left hand side in Fig. 3.3(b), were found in all the AAA specimens, and also in some cases, dramatic wall defects.
In contrast, the TAA specimens seemed in general more intact. Figure 3.2, shows the same signs of calcification and fiber remodeling but in a much earlier state than in the AAA specimen in Fig. 3.3. The content of elastin, shown in Fig. 3.2(d) as black fibers and smooth muscle cells, visible through the amount of cell cores in Fig. 3.2(b),was much higher.
These structural differences make sense in light of the difference in the mechanical parameters. The higher initial stiffness i.e. the stiffness in the low strain region, for the AAA tissue, represented by a higher k_1 parameter, corresponds to the collagen network that replaces the softer elastin matrix.
In all AAA specimens highly concentrated cell clusters, as shown on the right hand side of the tissue sample in Fig. 3.3(a) as an accumulation of black dots, indicate the presence of an inflammation, which were less common in the TAA specimens and if present, not as distinct. Inflammations could play a key role in the development and growth of aneurysms,

especially for AAA, according to Thompson (2005) and Shimizu et al. (2006).
For the thoracic specimens two samples in each direction were cut out and tested and overall they had similar properties, but in contrast for specimen T.2 the parameters k_1 and φ varied greatly. This could indicate the high heterogeneity of the tissue.
When measuring the thickness of the samples we found a high variation within the different samples, for the abdominal samples, the mean value was 2.12 mm $\pm$ 0.42 mm and for the thoracic samples 1.98 mm $\pm$ 0.3 mm. But also observed variation in the thickness within one tissue sample, exemplary given for the abdominal sample A.4, as 2.23 mm $\pm$ 0.46 mm (mean $\pm$ std of 4 measure points from one tested strip), which is in accordance with the results from Raghavan et al. (2006). These variance of thickness has an major influence on the reliability of rupture risk estimations based on simulated stress distributions, because of to the definition of stress, as force divide by area, the importance of accurate in-vivo thickness measuring is self-explaining, recent applications are e.g. MRT (Bartoli et al. 2012) or ultrasound (Duivenvoorden et al. 2009).

4.5. Limitations

A limitation of modeling biological tissue with an approach based on continuum mechanics is that no heterogeneities within the sample are considered, an assumption that could lead to inaccuracies especially in highly remodeled tissues like aneurysms. We also didn't consider the passive mechanical properties of smooth muscle cells within the tissue with our model, for the highly remodeled AAA samples the influence should be neglectable but not for TAA samples, where the muscle cells seemed mainly intact. For the in-vivo response neglecting smooth muscle cells would have an even higher effect on the accuracy because of the active response of the muscle cells i.e. contracting, which can only be taken into account when additionally biochemical processes are considered (Murtada et al. 2012). Also no long term behavior and biological responses can be predicted by a pure mechanical model, therefore growth models, e.g. by Satha et al. (2014)or remodeling models for collagen networks e.g. Hadi et al. (2012), where remodeling is simulated by an deterministic multi-scale mechanical model, must be considered for reliably reflecting the evolution of aneurysms due to physiological in-vivo loading until failure, due to tissue weakening, or stabilizing. Nevertheless for failure prediction and damage quantification due to supra-physiological loading, which is induced for example during balloon angioplasty but also could be caused by peak values of the blood pressure, the tissue response, immediately after the loading is applied, is of highest interest for failure and therefor the proposed model is sufficient.
A limitation of the procedure is that we performed uniaxial extension tests, although biaxial testing would mimic the in vivo loading condition better. The biaxial test was impossible to apply here due to the small size of the samples. Furthermore higher loads can be applied with uniaxial testing because the fixation with hooks, as used for the biaxial testing device, tends to rupture at comparatively low strains, in a manner not applicable to the current goals.

To the authors' best knowledge no data about the influence of storage at -20°C on the mechanical properties of human aneurysm tissue was available, unfortunately the only experiments with human tissue were performed by Adham et al. (1996) at -80°C and so it is not comparable with our study. Venkatasubramanian et al. (2006) investigated the changing mechanical behavior of aortic tissue from pigs due to freezing and came to the result that major changes are only evident in the low strain region of the mechanical response. But in contrast, Chow and Zhang (2011), who performed experiments on bovine aortic tissue, found no significant change in the low strain region but in the high strain region of the mechanical response. The conclusion is that there are most likely changes within the tissue due to intracellular ice formation but we are not able to estimate the influence on the mechanical properties of human aneurysm tissue.

Bibliography

Mustapha Adham, Jean-Paul Gournier, Jean-Pierre Favre, Eric De La Roche, Christian Ducerf, Jacques Baulieux, Xavier Barral, and Michel Pouyet. Mechanical characteristics of fresh and frozen human descending thoracic aorta, 1996.

Ali N. Azadani, Sam Chitsaz, Alex Mannion, Aart Mookhoek, Andrew Wisneski, Julius M. Guccione, Michael D. Hope, Liang Ge, and Elaine E. Tseng. Biomechanical properties of human ascending thoracic aortic aneurysms, 2013.

Pierre Badel, Stẽphane Avril, Michael A. Sutton, and Susan M. Lessner. Numerical simulation of arterial dissection during balloon angioplasty of atherosclerotic coronary arteries, 2014.

K. Balakhovsky, M. Jabareen, and K.Y. Volokh. Modeling rupture of growing aneurysms, 2014.

D. Balzani, J. Schröder, and D. Gross. Simulation of discontinuous damage incorporating residual stresses in circumferentially overstretched atherosclerotic arteries. *Acta Biomaterialia*, 2(6):609 – 618, 2006.

Daniel Balzani, Sarah Brinkhues, and Gerhard A. Holzapfel. Constitutive framework for the modeling of damage in collagenous soft tissues with application to arterial walls. *Computer Methods in Applied Mechanics and Engineering*, 213216(0):139 – 151, 2012.

M.A. Bartoli, F. Kober, P. Cozzone, R.W. Thompson, M.C. Alessi, and M. Bernard. In vivo assessment of murine elastase-induced abdominal aortic aneurysm with high resolution magnetic resonance imaging. *European Journal of Vascular and Endovascular Surgery*, 44(5):475 – 481, 2012.

Chen-Ket Chai, Ali C. Akyildiz, Lambert Speelman, Frank J.H. Gijsen, Cees W.J. Oomens, Marc R.H.M. van Sambeek, Aad van der Lugt, and Frank P.T. Baaijens. Local axial compressive mechanical properties of human carotid atherosclerotic plaquescharacterisation by indentation test and inverse finite element analysis. *Journal of Biomechanics*, 46(10): 1759 – 1766, 2013.

Ming-Jay Chow and Yanhang Zhang. Changes in the mechanical and biochemical properties of aortic tissue due to cold storage, 2011.

Eric de Groot, Sander I van Leuven, Raphael Duivenvoorden, Marijn C Meuwese, Fatima Akdim, Michiel L Bots, and John JP Kastelein. Measurement of carotid intima-media thickness to assess progression and regression of atherosclerosis. *Nat Clin Pract Cardiovasc Med*, 5(5):280–288, 2008.

R. Duivenvoorden, E. de Groot, B.M. Elsen, J.S. Laméris, R.J. van der Geest, E.S. Stroes, J.J.P. Kastelein, and A.J. Nederveen. In vivo quantification of carotid artery wall dimensions: 3.0-tesla mri versus b-mode ultrasound imaging. *Circulation: Cardiovascular Imaging*, 2(3):235–242, 2009.

Nele Famaey, Gerhard Sommer, Jos Vander Sloten, and Gerhard A. Holzapfel. Arterial clamping: Finite element simulation and in vivo validation. *Journal of the Mechanical Behavior of Biomedical Materials*, 12(0):107 – 118, 2012.

H.M. Finlay, L. McCullough, and P.B. Canham. Three-dimensional collagen organization of human brain arteries at different transmural pressures, 1995.

T. Christian Gasser. An irreversible constitutive model for fibrous soft biological tissue: A 3-d microfiber approach with demonstrative application to abdominal aortic aneurysms. *Acta Biomaterialia*, 7(6):2457 – 2466, 2011.

T. Christian Gasser, Ray W. Ogden, and Gerhard A. Holzapfel. Hyperelastic modelling of arterial layers with distributed collagen fibre orientations. *Journal of The Royal Society Interface*, 3(6):15–35, 2006.

M.F. Hadi, E.A. Sander, J.W. Ruberti, and V.H. Barocas. Simulated remodeling of loaded collagen networks via strain-dependent enzymatic degradation and constant-rate fiber growth. *Mechanics of Materials*, 44(0):72 – 82, 2012. Microstructures and Anisotropies.

Gerhard A. Holzapfel. Determination of material models for arterial walls from uniaxial extension tests and histological structure. *Journal of Theoretical Biology*, 238(2):290 – 302, 2006.

Gerhard A. Holzapfel, Thomas C. Gasser, and Ray W. Ogden. A new constitutive framework for arterial wall mechanics and a comparative study of material models. *Journal of elasticity and the physical science of solids*, 61(1-3):1–48, 2000.

J.D. Humphrey and G.A. Holzapfel. Mechanics, mechanobiology, and modeling of human abdominal aorta and aneurysms, 2012.

F. Iannaccone, N. Debusschere, S. De Bock, M. De Beule, D. Van Loo, F. Vermassen, P. Segers, and B. Verhegghe. The influence of vascular anatomy on carotid artery stenting: A parametric study for damage assessment, 2014.

Adrien Kaladji, Aurlien Dumenil, Miguel Castro, Alain Cardon, Jean-Pierre Becquemin, Benyebka Bou-Sad, Antoine Lucas, and Pascal Haigron. Prediction of deformations during endovascular aortic aneurysm repair using finite element simulation. *Computerized Medical Imaging and Graphics*, 37(2):142 – 149, 2013. Special Issue on Mixed Reality Guidance of Therapy - Towards Clinical Implementation.

Atsushi Kitagawa, Tara M. Mastracci, Regula von Allmen, and Janet T. Powell. The role of diameter versus volume as the best prognostic measurement of abdominal aortic aneurysms, 2013.

H.W. Kniemeyer, T. Kessler, P.U. Reber, H.B. Ris, H. Hakki, and M.K. Widmer. Treatment of ruptured abdominal aortic aneurysm, a permanent challenge or a waste of resources? prediction of outcome using a multi-organ-dysfunction score, 2000.

Frank A. Lederle, Samuel E. Wilson, Gary R. Johnson, Donovan B. Reinke, Fred N. Littooy, Charles W. Acher, David J. Ballard, Louis M. Messina, Ian L. Gordon, Edmund P. Chute, William C. Krupski, Steven J. Busuttil, Gary W. Barone, Steven Sparks, Linda M. Graham, Joseph H. Rapp, Michel S. Makaroun, Gregory L. Moneta, Robert A. Cambria, Raymond G. Makhoul, Darwin Eton, Howard J. Ansel, Julie A. Freischlag, and Dennis Bandyk. Immediate repair compared with surveillance of small abdominal aortic aneurysms. *New England Journal of Medicine*, 346(19):1437–1444, 2002.

Jan H. N. Lindeman, Brian A. Ashcroft, Jan-Willem M. Beenakker, Maarten van Es, Nico B. R. Koekkoek, Frans A. Prins, Jarl F. Tielemans, Hazem Abdul-Hussien, Ruud A. Bank, and Tjerk H. Oosterkamp. Distinct defects in collagen microarchitecture underlie vessel-wall failure in advanced abdominal aneurysms and aneurysms in marfan syndrome. *Proceedings of the National Academy of Sciences*, 107(2):862–865, 2010.

R. Luengo-Fernandez J. Leal A. Gray P. Scarborough M. Rayner M. Nichols, N. Townsend. European cardiovascular disease statistics 2012. *European Heart Network and European Society of Cardiology*, 2012.

Caitlin Martin, Wei Sun, Thuy Pham, and John Elefteriades. Predictive biomechanical analysis of ascending aortic aneurysm rupture potential. *Acta Biomaterialia*, 9(12):9392 – 9400, 2013.

Karol Miller and Jia Lu. On the prospect of patient-specific biomechanics without patient-specific properties of tissues. *Journal of the Mechanical Behavior of Biomedical Materials*, 27(0):154 – 166, 2013.

Peter Mortier, Gerhard A. Holzapfel, Matthieu Beule, Denis Loo, Yves Taeymans, Patrick Segers, Pascal Verdonck, and Benedict Verhegghe. A novel simulation strategy for stent insertion and deployment in curved coronary bifurcations: Comparison of three drug-eluting stents. *Annals of Biomedical Engineering*, 38(1):88–99, 2010.

J.J. Mulvihill, E.M. Cunnane, S.M. McHugh, E.G. Kavanagh, S.R. Walsh, and M.T. Walsh. Mechanical, biological and structural characterization of in vitro ruptured human carotid plaque tissue. *Acta Biomaterialia*, 9(11):9027 – 9035, 2013.

Saeil C. Murtada, Anders Arner, and Gerhard A. Holzapfel. Experiments and mechanochemical modeling of smooth muscle contraction: Significance of filament overlap. *Journal of Theoretical Biology*, 297(0):176 – 186, 2012.

R. W. Ogden and D. G. Roxburgh. A pseudoelastic model for the mullins effect in filled rubber. *Proceedings of the Royal Society of London. Series A: Mathematical, Physical and Engineering Sciences*, 455(1988):2861–2877, 1999.

Estefania Peña, Juan A. Peña, and Manuel Doblaré. On the mullins effect and hysteresis of fibered biological materials: A comparison between continuous and discontinuous damage models. *International Journal of Solids and Structures*, 46(78):1727 – 1735, 2009.

T. Pham, C. Martin, J. Elefteriades, and W. Sun. Biomechanical characterization of ascending aortic aneurysm with concomitant bicuspid aortic valve and bovine aortic arch. *Acta Biomaterialia*, 9(8):7927 – 7936, 2013.

Madhavan L. Raghavan, Jarin Kratzberg, Erasmo Magalhães Castro de Tolosa, Mauro M. Hanaoka, Patricia Walker, and Erasmo Simão da Silva. Regional distribution of wall thickness and failure properties of human abdominal aortic aneurysm, 2006.

Samarth S. Raut, Santanu Chandra, Judy Shum, and Ender A. Finol. The role of geometric and biomechanical factors in abdominal aortic aneurysm rupture risk assessment. *Annals of Biomedical Engineering*, 41(7):1459–1477, 2013.

S.R. Rickaby and N.H. Scott. A model for the mullins effect during multicyclic equibiaxial loading. *Acta Mechanica*, 224(9):1887–1900, 2013.

S. Roccabianca, C.A. Figueroa, G. Tellides, and J.D. Humphrey. Quantification of regional differences in aortic stiffness in the aging human. *Journal of the Mechanical Behavior of Biomedical Materials*, 29(0):618 – 634, 2014.

José F. Rodríguez, Fernando Cacho, José A. Bea, and Manuel Doblaré. A stochastic-structurally based three dimensional finite-strain damage model for fibrous soft tissue. *Journal of the Mechanics and Physics of Solids*, 54(4):864 – 886, 2006.

José F. Rodríguez, Gerhard A. Holzapfel, Cristina Ruiz, and Manuel Doblaré. Mechanical stresses in abdominal aortic aneurysms: Influence of diameter, asymmetry, and material anisotropy. *Journal of Biomechanical Engineering*, 130(2):021023–021023, 2008.

José F. Rodríguez, Giampalo Martufi, Manuel Doblaré, and Ender A. Finol. The effect of material model formulation in the stress analysis of abdominal aortic aneurysms. *Annals of Biomedical Engineering*, 37(11):2218–2221, 2009.

Aaron Romo, Pierre Badel, Ambroise Duprey, Jean-Pierre Favre, and Stéphane Avril. In vitro analysis of localized aneurysm rupture, 2014.

Ganarupan Satha, StefanB. Lindström, and Anders Klarbring. A goal function approach to remodeling of arteries uncovers mechanisms for growth instability. *Biomechanics and Modeling in Mechanobiology*, pages 1–17, 2014.

Andreas J. Schriefl, Georg Zeindlinger, David M. Pierce, Peter Regitnig, and Gerhard A. Holzapfel. Determination of the layer-specific distributed collagen fibre orientations in human thoracic and abdominal aortas and common iliac arteries. *Journal of The Royal Society Interface*, 2011.

Andreas J. Schriefl, Heimo Wolinski, Peter Regitnig, Sepp D. Kohlwein, and Gerhard A. Holzapfel. An automated approach for three-dimensional quantification of fibrillar structures in optically cleared soft biological tissues. *Journal of The Royal Society Interface*, 10(80), 2013.

Koichi Shimizu, Richard N. Mitchell, and Peter Libby. Inflammation and cellular immune responses in abdominal aortic aneurysms. *Arteriosclerosis, Thrombosis, and Vascular Biology*, 26(5):987–994, 2006.

Dimitrios P. Sokolis, Eleftherios P. Kritharis, and Dimitrios C. Iliopoulos. Effect of layer heterogeneity on the biomechanical properties of ascending thoracic aortic aneurysms. *Medical & Biological Engineering & Computing*, 50(12):1227–1237, 2012.

Yoriyasu Suzuki, Fumiaki Ikeno, Tomomi Koizumi, Fermin Tio, Alan C. Yeung, Paul G. Yock, Peter J. Fitzgerald, and William F. Fearon. In vivo comparison between optical coherence tomography and intravascular ultrasound for detecting small degrees of in-stent neointima after stent implantation. *JACC: Cardiovascular Interventions*, 1(2):168 – 173, 2008.

Robert W Thompson. Aneurysm treatments expand. *Nat Med*, 11(12):1279–1281, 2005.

Lucas H Timmins, Matthew W Miller, Fred J Clubb, and James E Moore. Increased artery wall stress post-stenting leads to greater intimal thickening. *Lab Invest*, 91(6):955–967, 2011.

J. Tong, T. Cohnert, P. Regitnig, and G.A. Holzapfel. Effects of age on the elastic properties of the intraluminal thrombus and the thrombus-covered wall in abdominal aortic aneurysms: Biaxial extension behaviour and material modelling, 2011.

J. Tong, T. Cohnert, P. Regitnig, J. Kohlbacher, R. Birner-Gruenberger, A.J. Schriefl, G. Sommer, and G.A. Holzapfel. Variations of dissection properties and mass fractions with thrombus age in human abdominal aortic aneurysms, 2014.

Alkiviadis Tsamis, Jeffrey T. Krawiec, and David A. Vorp. Elastin and collagen fibre microstructure of the human aorta in ageing and disease: a review. *Journal of The Royal Society Interface*, 10(83), 2013.

Gijs van Soest, Senada Koljenovi, Brett E. Bouma, Guillermo J. Tearney, J. Wolter Oosterhuis, Patrick W. Serruys, Anton F. W. van der Steen, Nieves Gonzalo, Sander van Noorden, Geert L. J. H. van Leenders, Thad Goderie, Evelyn Regar, and Takayuki Okamura. Atherosclerotic tissue characterization in vivo by optical coherence tomography attenuation imaging. *Journal of Biomedical Optics*, 15(1):011105–011105–9, 2010.

Jonathan P. Vande Geest, Michael S. Sacks, and David A. Vorp. The effects of aneurysm on the biaxial mechanical behavior of human abdominal aorta, 2006.

Jonathan P. Vande Geest, David E. Schmidt, Michael S. Sacks, and David A. Vorp. The effects of anisotropy on the stress analyses of patient-specific abdominal aortic aneurysms. *Annals of Biomedical Engineering*, 36(6):921–932, 2008.

Ramji T. Venkatasubramanian, Erin D. Grassl, Victor H. Barocas, Daniel Lafontaine, and John C. Bischof. Effects of freezing and cryopreservation on the mechanical properties of arteries. *Annals of Biomedical Engineering*, 34(5):823–832, 2006.

K.Y. Volokh and D.A. Vorp. A model of growth and rupture of abdominal aortic aneurysm, 2008.

David A. Vorp. Biomechanics of abdominal aortic aneurysm. *Journal of Biomechanics*, 40(9):1887 – 1902, 2007.

Hannah Weisbecker, David M. Pierce, Peter Regitnig, and Gerhard A. Holzapfel. Layer-specific damage experiments and modeling of human thoracic and abdominal aortas with non-atherosclerotic intimal thickening. *Journal of the Mechanical Behavior of Biomedical Materials*, 12(0):93 – 106, 2012.

J. S. Wilson, S. Baek, and J. D. Humphrey. Importance of initial aortic properties on the evolving regional anisotropy, stiffness and wall thickness of human abdominal aortic aneurysms. *Journal of The Royal Society Interface*, 9(74):2047–2058, 2012.

Meiting Wu, Cameron Rementer, and Cecilia M. Giachelli. Vascular calcification: An update on mechanisms and challenges in treatment. *Calcified Tissue International*, 93 (4):365–373, 2013.

Deutsche Fassung:
Beschluss der Curricula-Kommission für Bachelor-, Master- und Diplomstudien vom 10.11.2008
Genehmigung des Senates am 1.12.2008

EIDESSTATTLICHE ERKLÄRUNG

Ich erkläre an Eides statt, dass ich die vorliegende Arbeit selbstständig verfasst, andere als die angegebenen Quellen/Hilfsmittel nicht benutzt, und die den benutzten Quellen wörtlich und inhaltlich entnommenen Stellen als solche kenntlich gemacht habe.

Graz, am …… ……..
(Unterschrift)

Englische Fassung:

STATUTORY DECLARATION

I declare that I have authored this thesis independently, that I have not used other than the declared sources / resources, and that I have explicitly marked all material which has been quoted either literally or by content from the used sources.

…… ……..
date (signature)

A. Additional patient specific data

Donor -	Hypertension -	Diabetic -	Hypercolesteroma -	Smoking history -	Drinking W/B/C per Week	Caffeine cups/d	Sport h/week
Thoracic aorta							
T.1	1	1	1	0	0/0/0	2	0
T.2	3	0	2	0	2/0/0	2	0
T.3	1	0	0	0	0/0/0	0	0
T.4	2	0	2	0	-	-	-
T.5	0	0	0	0	-	-	-
Abdominal aorta							
A.1	1	1	1	-	0/7/0	5	0
A.2	1	0	1	0	2/2/0	5	0
A.3	1	0	1	0	0/3/0	5	0
A.4	1	1	1	1	2/0/0	5	0
A.5	1	0	1	2	0/0/0	5	0
A.6	1	0	1	0	0/0/0	5	2
A.7	1	0	1	1	3/2/0	1	5
A.8	1	0	1	0	-	5	0

Table A.1.: Patient medical background and lifestyle data. In columns 'Hypertension', 'Diabetic' and 'Hypercholesteroma' 0 stands for no diagnosis, 1 or higher means that the disease was detected and treated with the amount of different medications given by the number. A 0 in 'Smoking history' means that the patient never smoked or stopped more then 10 years ago, 1 means stopped in the last 10 years and 2 means smoking less then on pack a day. W/B/C stands for wine, beer and cocktails with the corresponding amount per day in the column. The consume of 'Caffeine' is also given in cups/day. In the last column the weekly hours of sport done by the patient are given.

B. Measured sample thicknesses

Toracic aorta												
	axial						circumferential					
Sample	1	2	3	4	mean	std.	1	2	3	4	mean	std.
	mm	mm	mm	mm	mm	mm	mm	mm	mm	mm	mm	mm
T.1.1	1.55	1.88	2.19	1.90	1.88	0.26	2.00	1.85	1.99	1.70	1.89	0.14
T.1.2	1.37	1.74	1.52	1.76	1.60	0.19	1.92	1.57	1.70	1.60	1.70	0.16
T.2.1	1.75	1.76	2.00	1.80	1.83	0.12	2.30	2.40	2.50	2.59	2.45	0.13
T.2.2	2.30	2.10	1.80	1.97	2.04	0.21	2.30	1.80	1.97	-	2.02	0.25
T.3.1	2.10	1.96	1.86	1.84	1.94	0.12	2.30	2.20	2.00	2.06	2.14	0.14
T.3.2	2.16	1.98	2.14	1.83	2.03	0.15	1.89	2.05	2.05	2.00	2.00	0.08
T.4.1	2.50	2.50	2.50	2.60	2.53	0.05	2.40	2.30	2.46	2.37	2.38	0.07
T.4.2	2.50	2.20	2.40	2.30	2.35	0.13	2.46	2.48	2.40	2.44	2.45	0.03
T.5.1	1.63	1.63	1.68	1.55	1.62	0.05	1.66	1.72	1.70	1.85	1.73	0.08
T.5.2	1.62	1.71	1.70	1.62	1.66	0.05	1.83	1.57	1.68	1.48	1.64	0.15
T.6.1	2.20	2.30	2.15	2.25	2.23	0.06	2.15	2.14	2.10	2.20	2.15	0.04
Abdominal aorta												
	axial						circumferential					
Sample	1	2	3	4	mean	std.	1	2	3	4	mean	std.
	mm	mm	mm	mm	mm	mm	mm	mm	mm	mm	mm	mm]
A.1	1.70	2.50	2.70	2.00	2.23	0.46	2.70	1.90	1.46	2.28	2.09	0.53
A.2	2.50	2.03	2.60	1.99	2.28	0.31	2.32	2.14	2.30	2.16	2.23	0.09
A.3	1.70	1.60	1.90	1.60	1.70	0.14	1.78	1.99	2.10	1.64	1.88	0.21
A.4	3.20	2.60	3.40	3.30	3.13	0.36	2.40	2.20	2.10	2.30	2.25	0.13
A.5	2.80	2.70	3.00	2.75	2.81	0.13	2.70	2.67	2.44	2.60	2.60	0.12
A.6	2.30	1.72	2.30	1.60	1.98	0.37	2.05	1.70	2.00	2.00	1.94	0.16
A.7	1.80	1.70	2.30	1.79	1.90	0.27	1.74	1.75	1.72	2.70	1.98	0.48
A.8.1	1.90	1.20	1.60	1.25	1.49	0.33	1.61	1.60	1.70	1.58	1.62	0.05
A.8.2	1.70	1.24	1.43	1.77	1.54	0.25	2.20	1.68	2.17	1.35	1.85	0.41

Table B.1.: Thicknesses of the tested specimens, measured at four evenly distributed locations (1-4), from the axially and circumferentially oriented testing strips with the calculated mean values and standard deviations

C. Histological images and plots of the fitted data

In this section images of the three different histological stainings and plots of the elastic and the stress-strain response, from the testing and the corresponding modeled values and the evolution of the minimum of the damage variable versus the stretch are shown for all samples tested.

Figure C.1.: Sample A.1

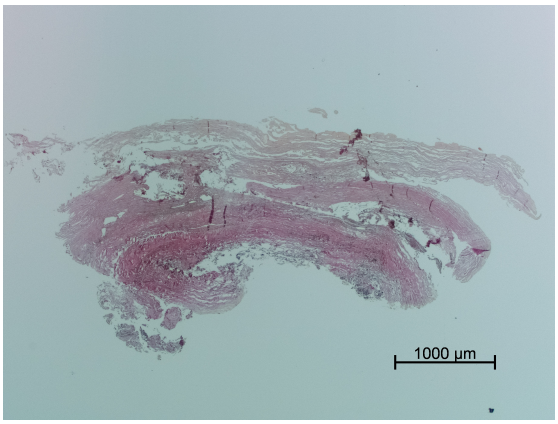

(a) Elastica van Gieson staining

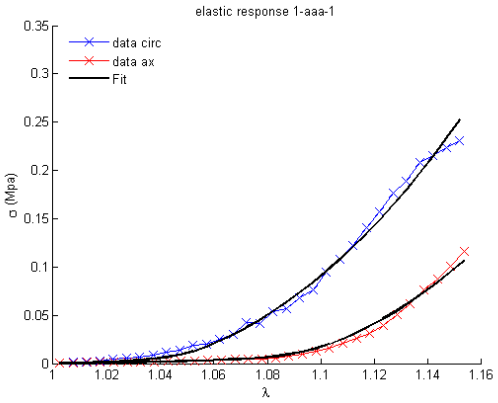

(b) Fitted elastic response

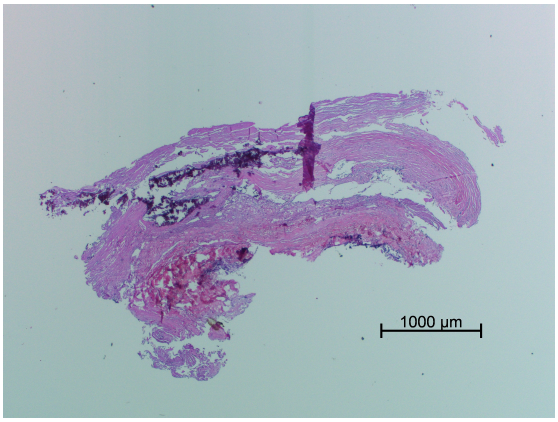

(c) Hematoxylin and eosin staining

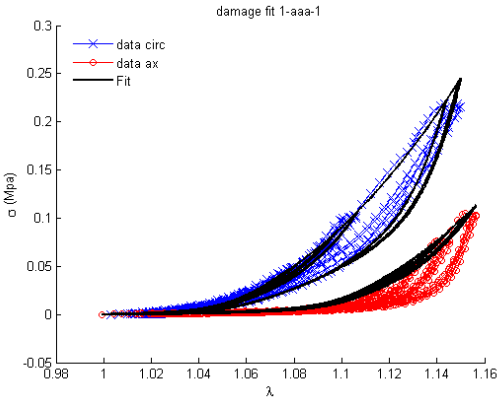

(d) Stress-strain response from mechanical testing and fitted response

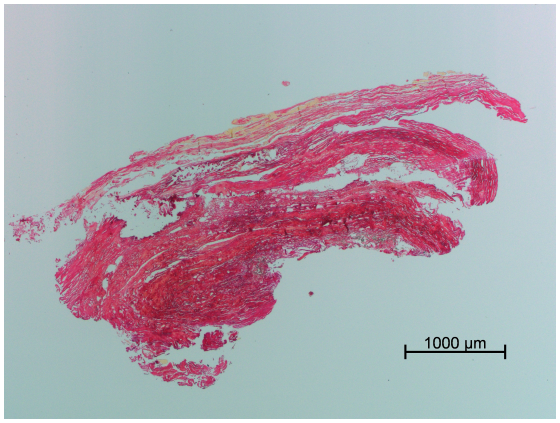

(e) Picosirius red staining

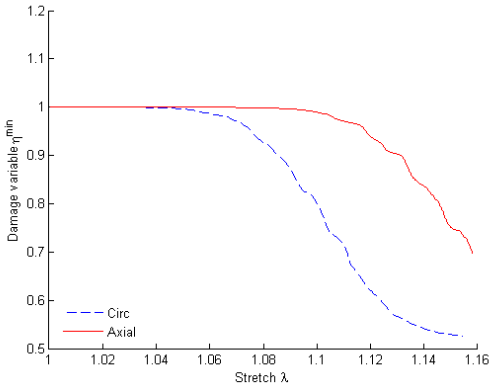

(f) Evolution of the damage variable vs. stretch

Figure C.2.: Sample A.2

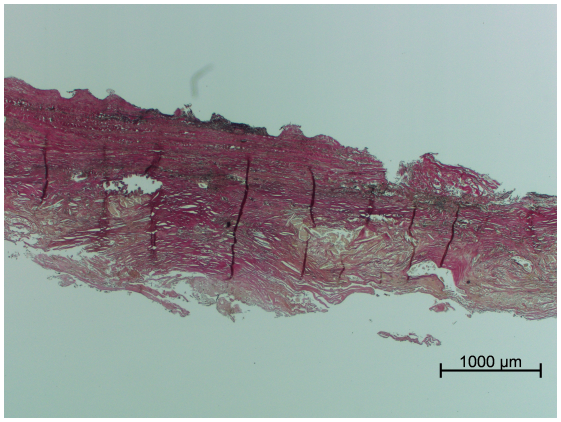

(a) Elastica van Gieson staining

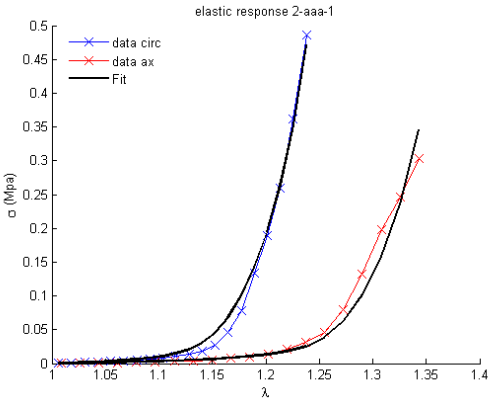

(b) Fitted elastic response

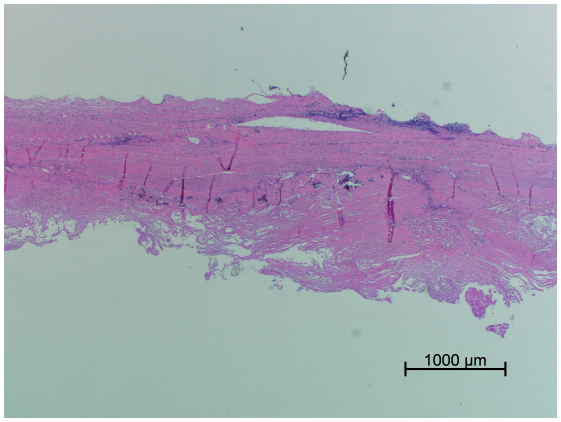

(c) Hematoxylin and eosin staining

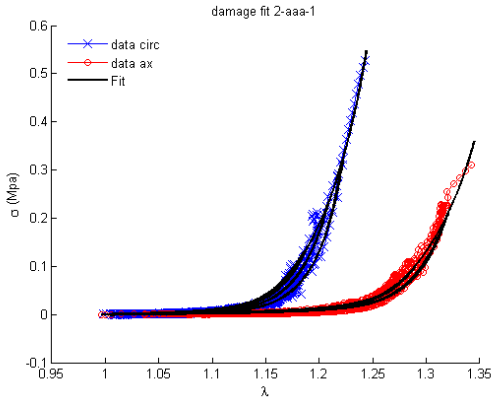

(d) Stress-strain response from mechanical testing and fitted response

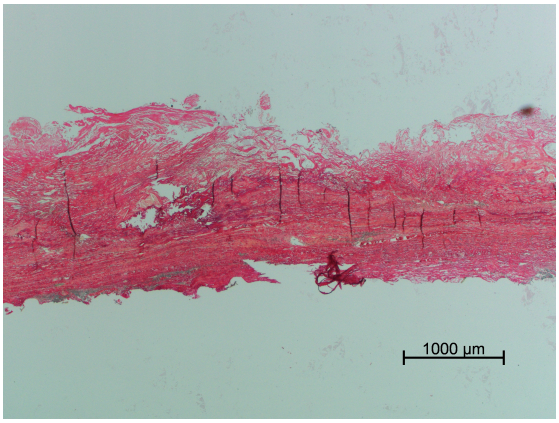

(e) Picosirius red staining

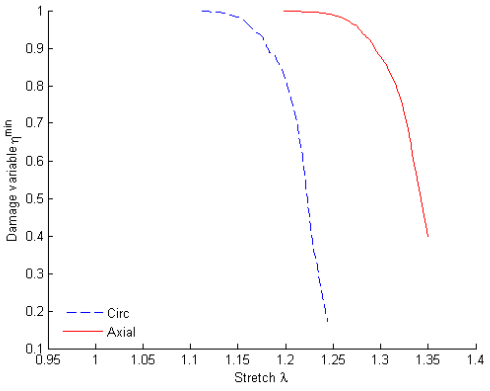

(f) Evolution of the damage variable vs. stretch

Figure C.3.: Sample A.3

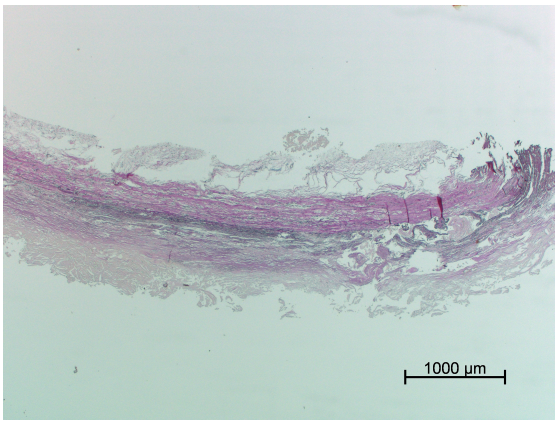

(a) Elastica van Gieson staining

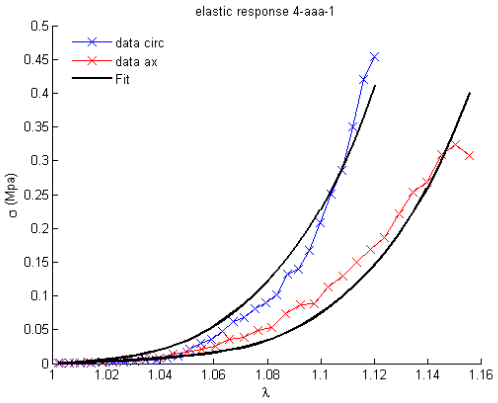

(b) Fitted elastic response

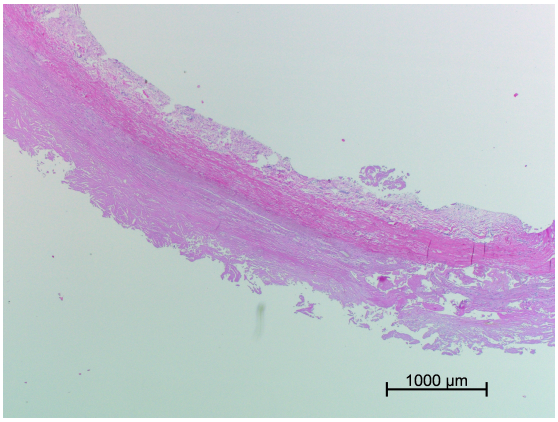

(c) Hematoxylin and eosin staining

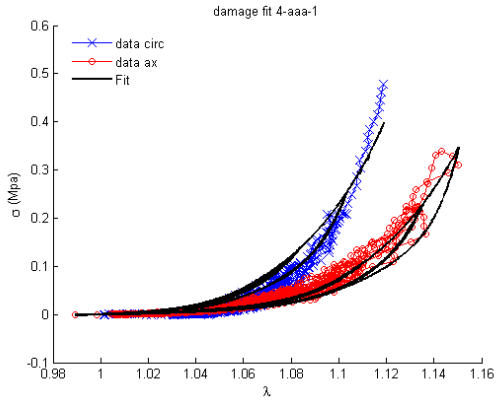

(d) Stress-strain response from mechanical testing and fitted response

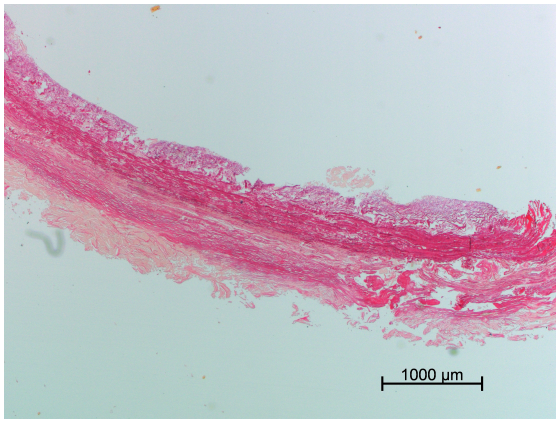

(e) Picosirius red staining

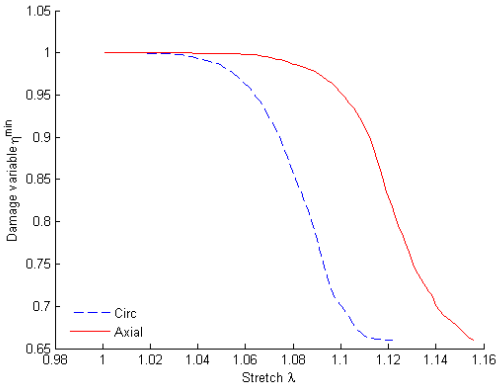

(f) Evolution of the damage variable vs. stretch

Figure C.4.: Sample A.4

(a) Elastica van Gieson staining

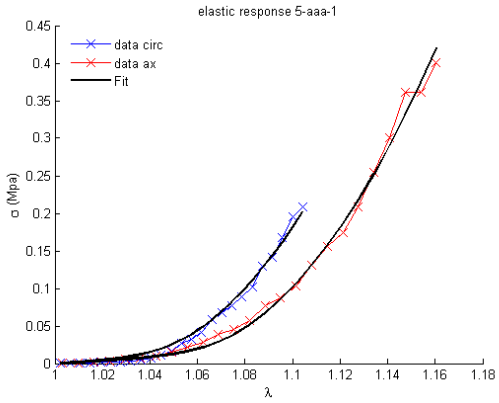

(b) Fitted elastic response

(c) Hematoxylin and eosin staining

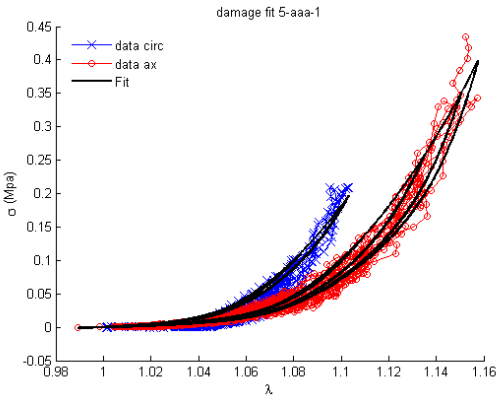

(d) Stress-strain response from mechanical testing and fitted response

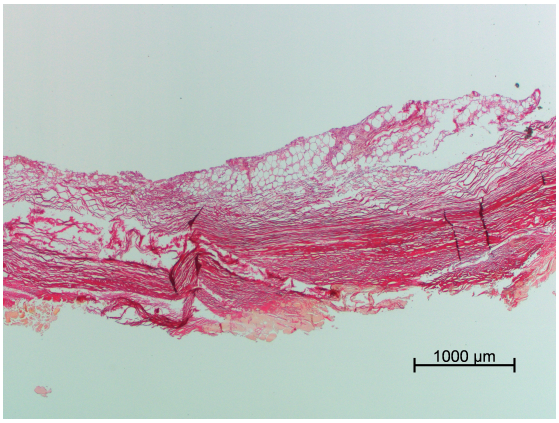

(e) Picosirius red staining

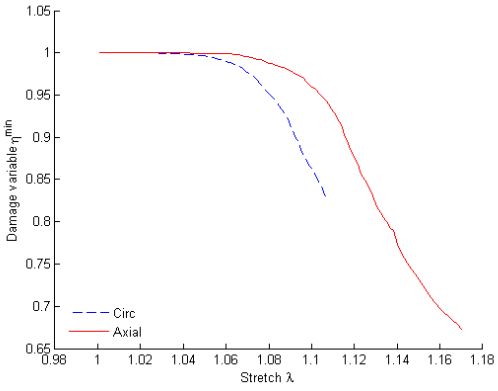

(f) Evolution of the damage variable vs. stretch

Figure C.5.: Sample A.5

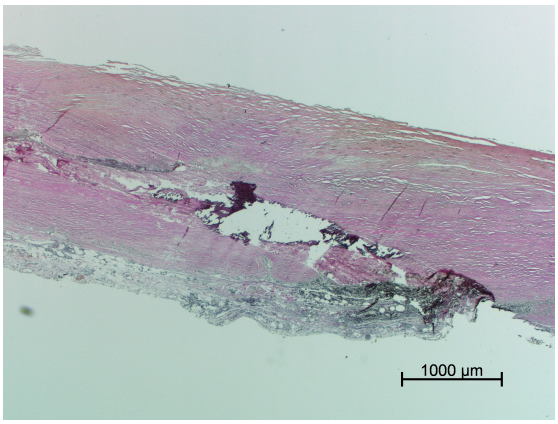

(a) Elastica van Gieson staining

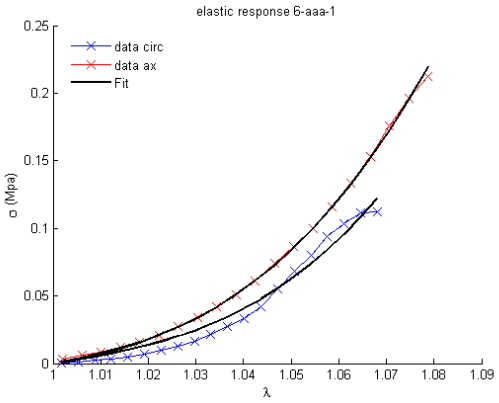

(b) Fitted elastic response

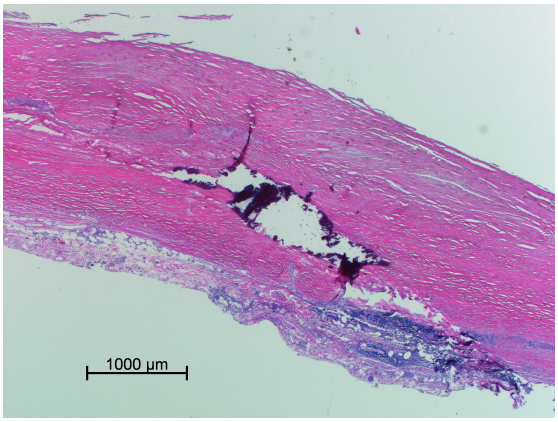

(c) Hematoxylin and eosin staining

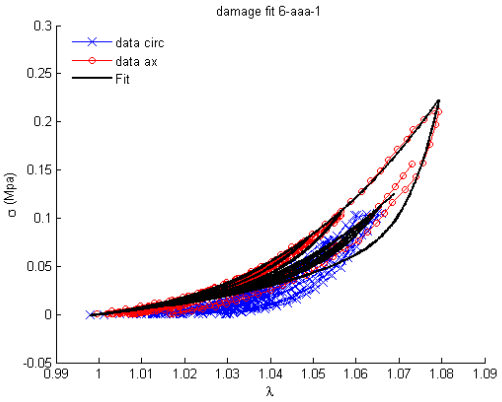

(d) Stress-strain response from mechanical testing and fitted response

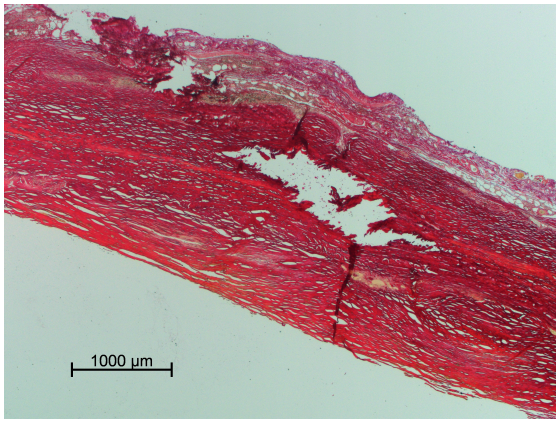

(e) Picosirius red staining

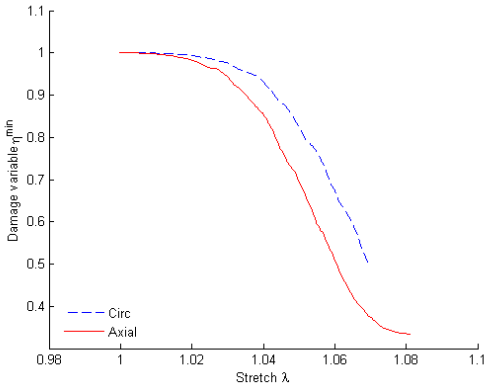

(f) Evolution of the damage variable vs. stretch

Figure C.6.: Sample A.6

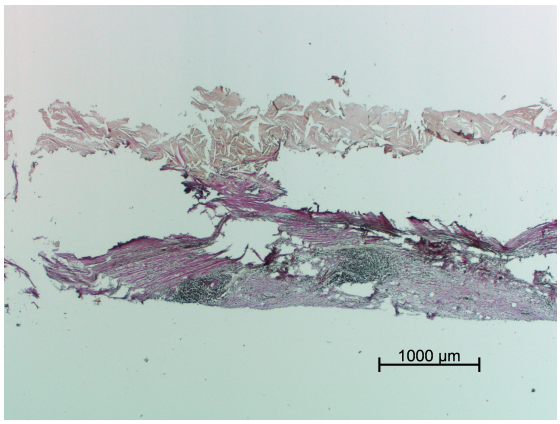

(a) Elastica van Gieson staining

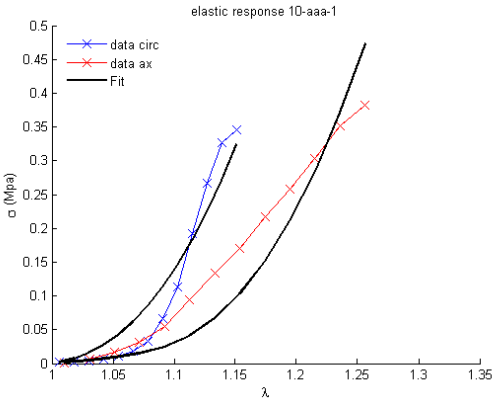

(b) Fitted elastic response

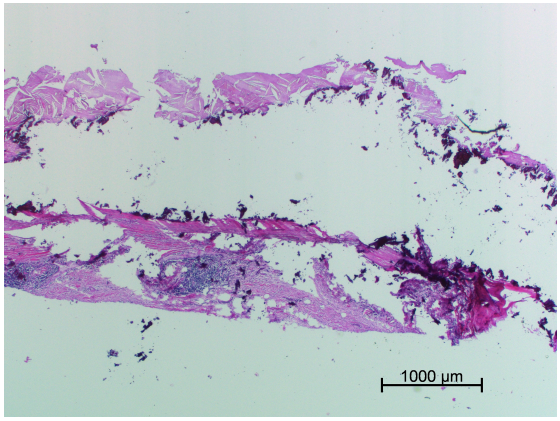

(c) Hematoxylin and eosin staining

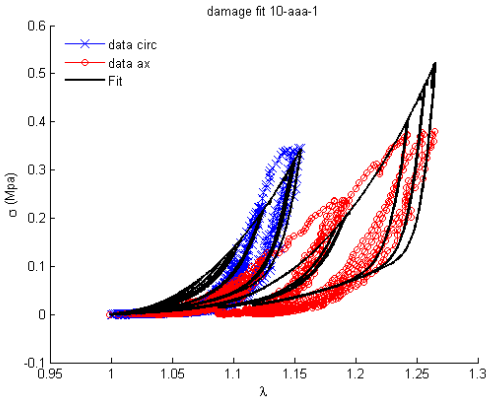

(d) Stress-strain response from mechanical testing and fitted response

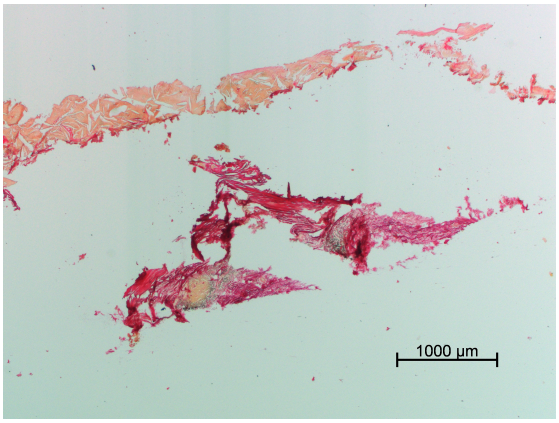

(e) Picosirius red staining

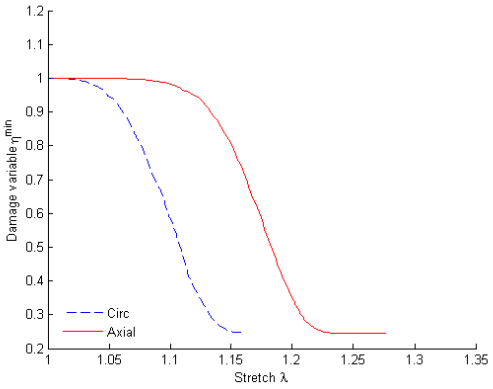

(f) Evolution of the damage variable vs. stretch

Figure C.7.: Sample A.7

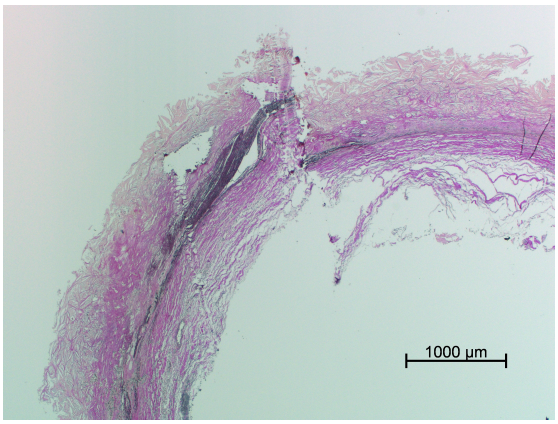

(a) Elastica van Gieson staining

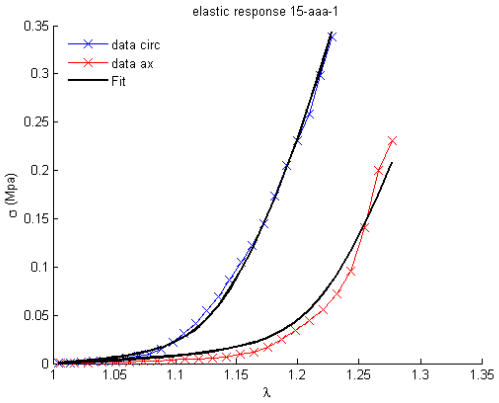

(b) Fitted elastic response

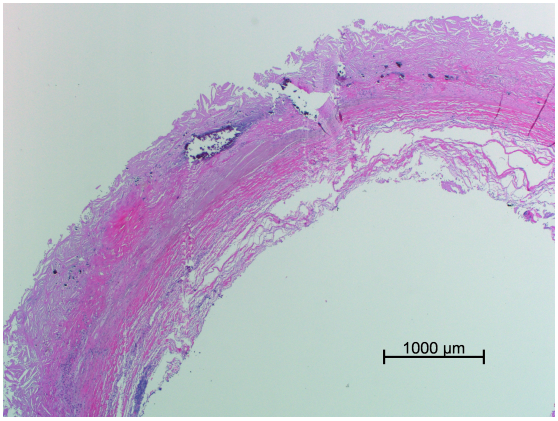

(c) Hematoxylin and eosin staining

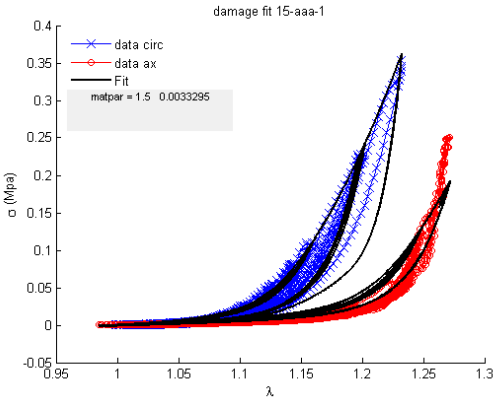

(d) Stress-strain response from mechanical testing and fitted response

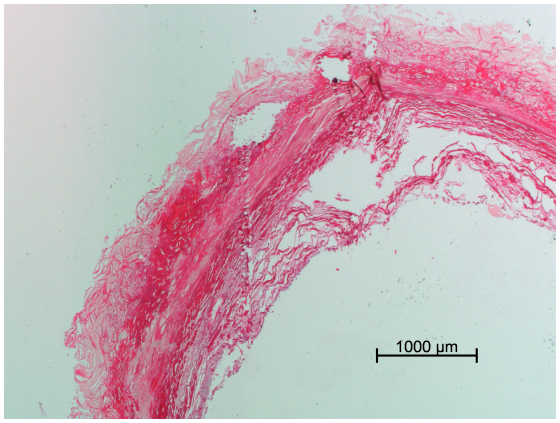

(e) Picosirius red staining

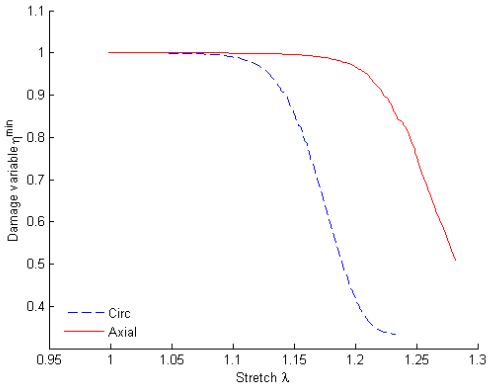

(f) Evolution of the damage variable vs. stretch

Figure C.8.: Sample A.8.1

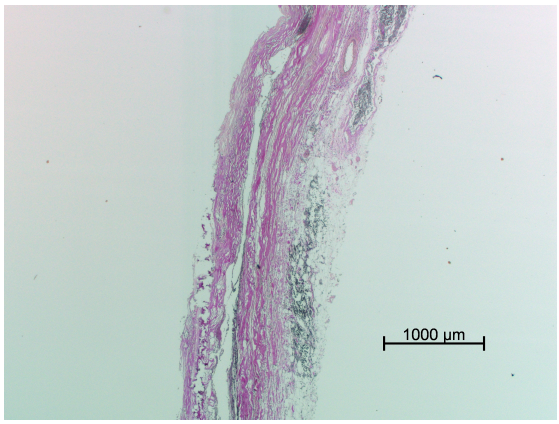

(a) Elastica van Gieson staining

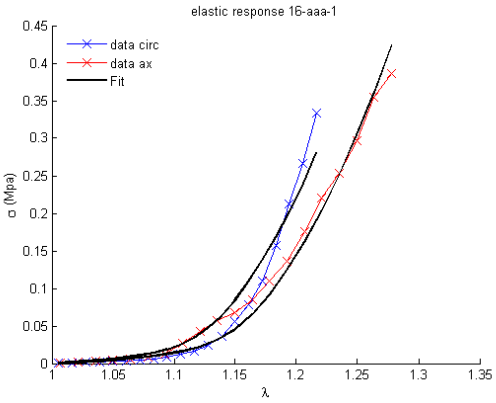

(b) Fitted elastic response

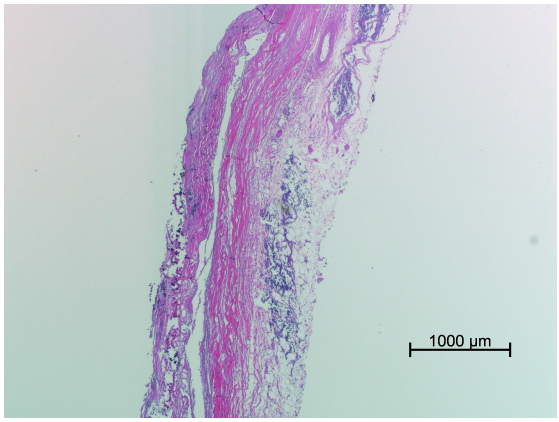

(c) Hematoxylin and eosin staining

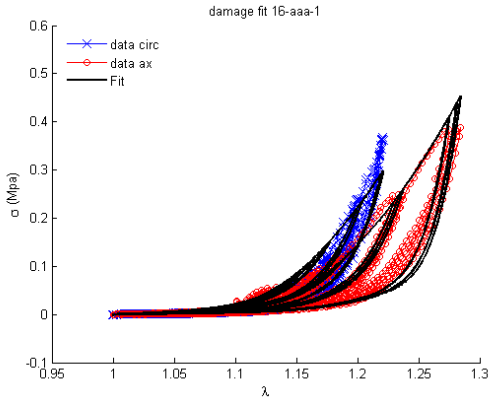

(d) Stress-strain response from mechanical testing and fitted response

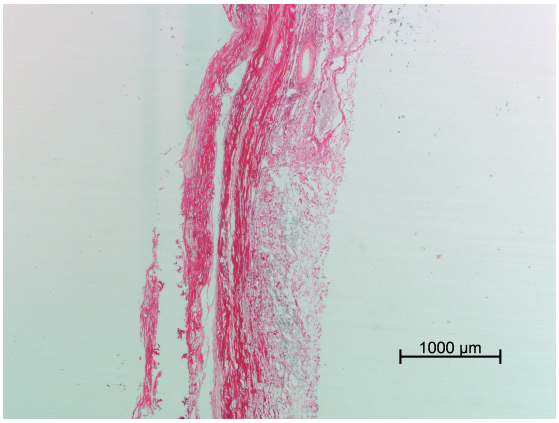

(e) Picosirius red staining

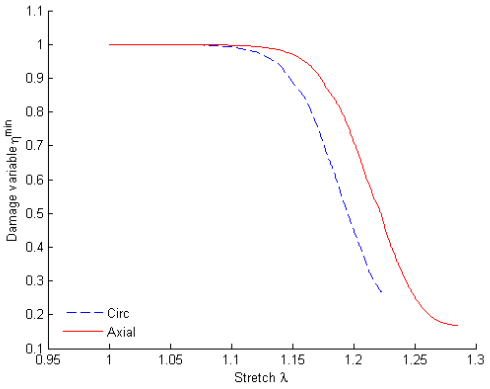

(f) Evolution of the damage variable vs. stretch

Figure C.9.: Sample A.8.2

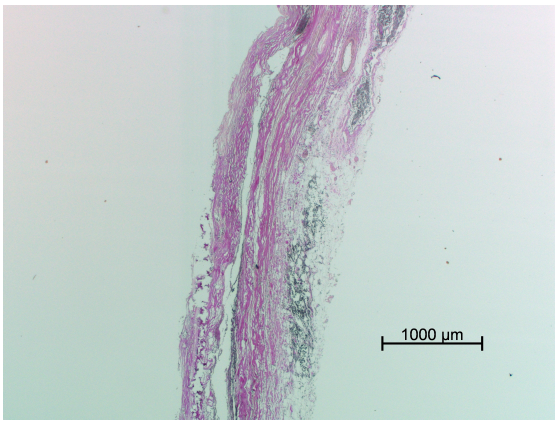

(a) Elastica van Gieson staining

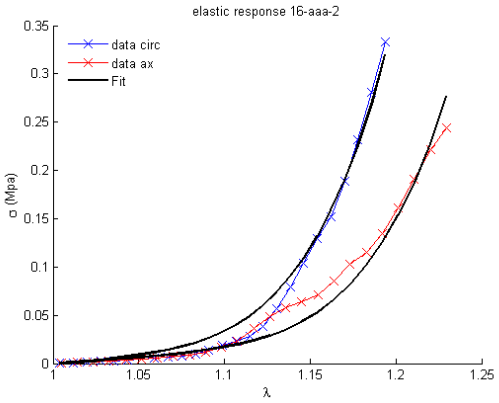

(b) Fitted elastic response

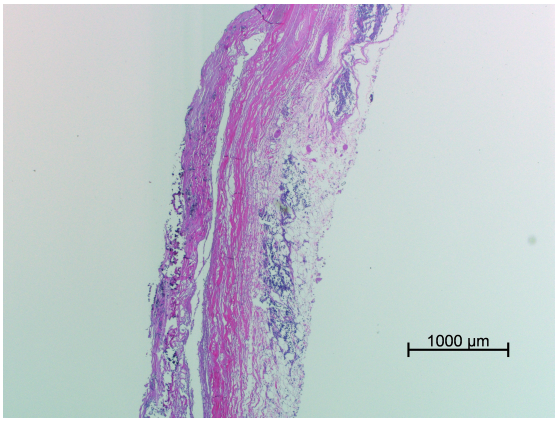

(c) Hematoxylin and eosin staining

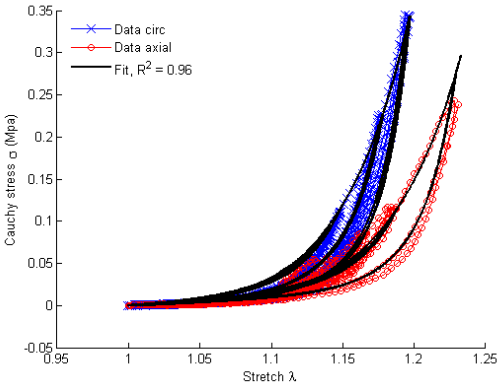

(d) Stress-strain response from mechanical testing and fitted response

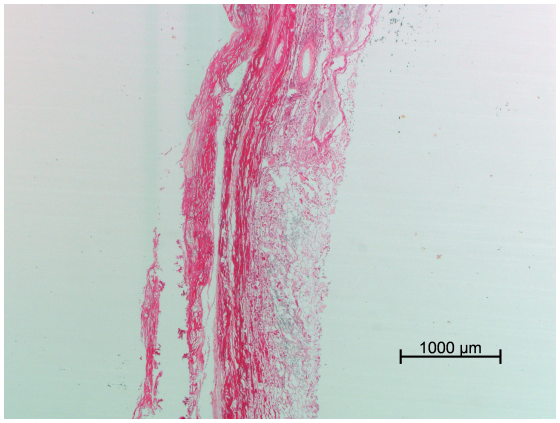

(e) Picosirius red staining

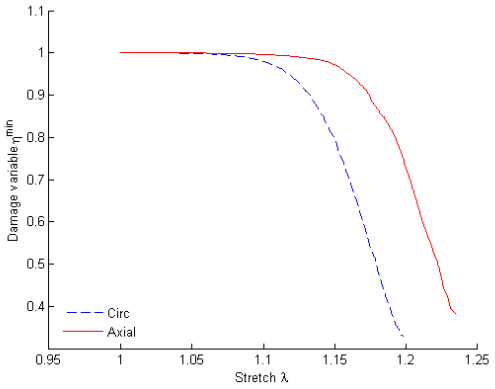

(f) Evolution of the damage variable vs. stretch

Figure C.10.: Sample T.1.1

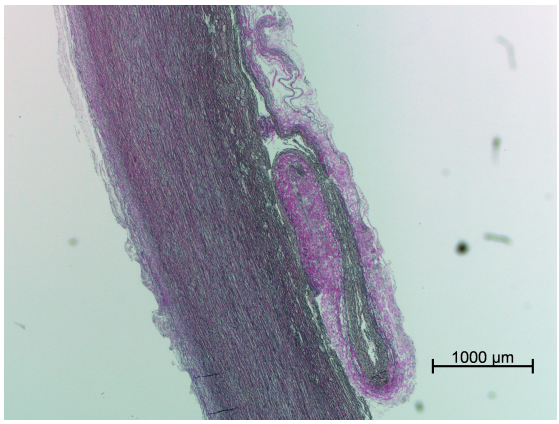

(a) Elastica van Gieson staining

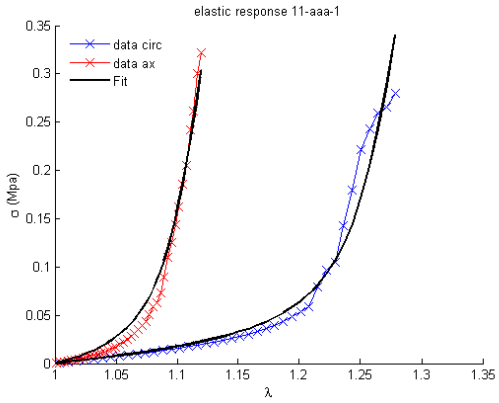

(b) Fitted elastic response

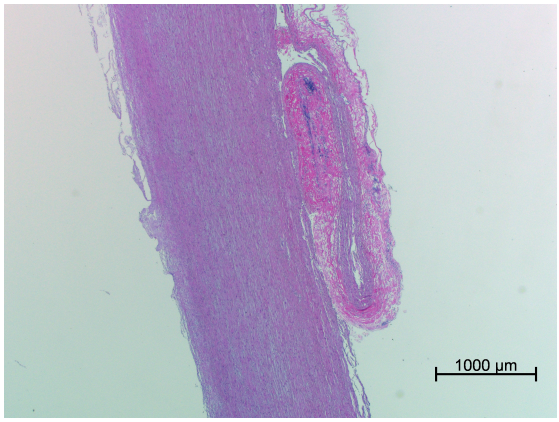

(c) Hematoxylin and eosin staining

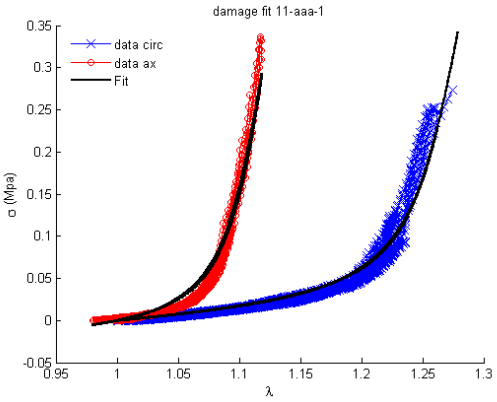

(d) Stress-strain response from mechanical testing and fitted response

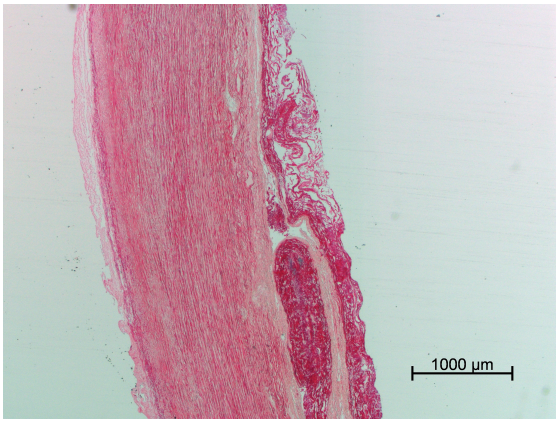

(e) Picosirius red staining

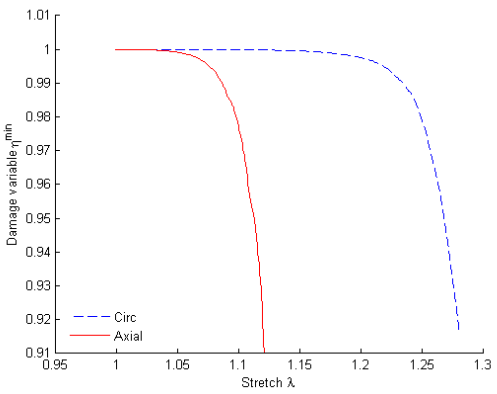

(f) Evolution of the damage variable vs. stretch

Figure C.11.: Sample T.1.2

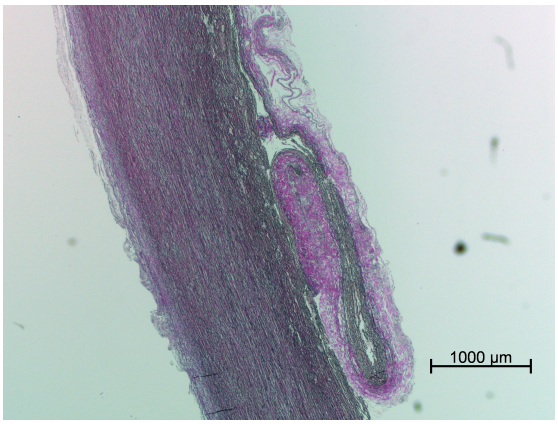

(a) Elastica van Gieson staining

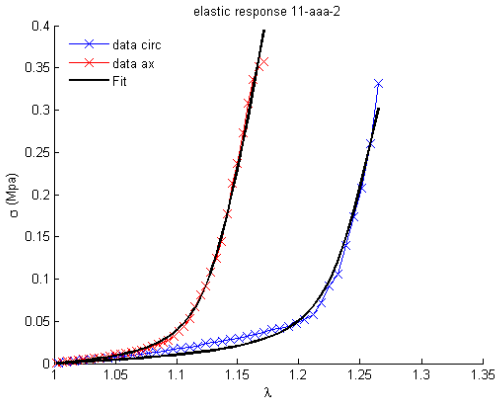

(b) Fitted elastic response

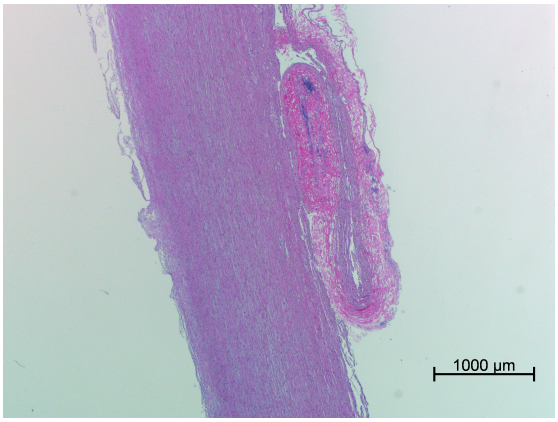

(c) Hematoxylin and eosin staining

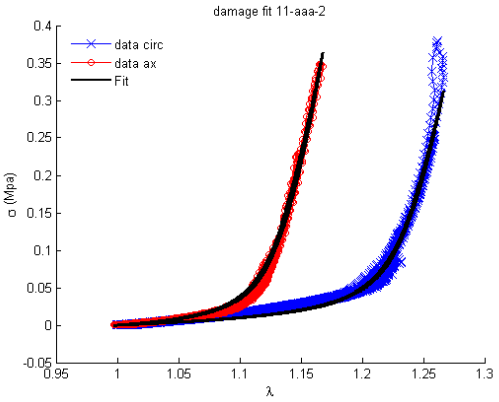

(d) Stress-strain response from mechanical testing and fitted response

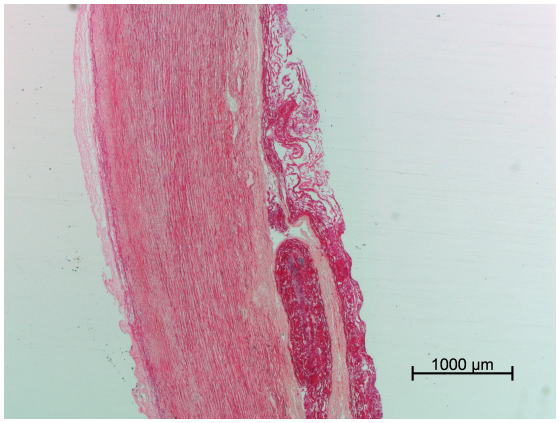

(e) Picosirius red staining

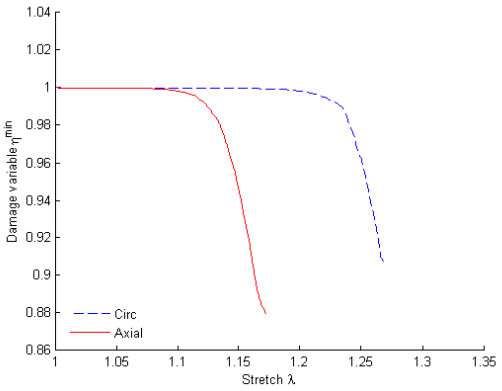

(f) Evolution of the damage variable vs. stretch

Figure C.12.: Sample T.2.1

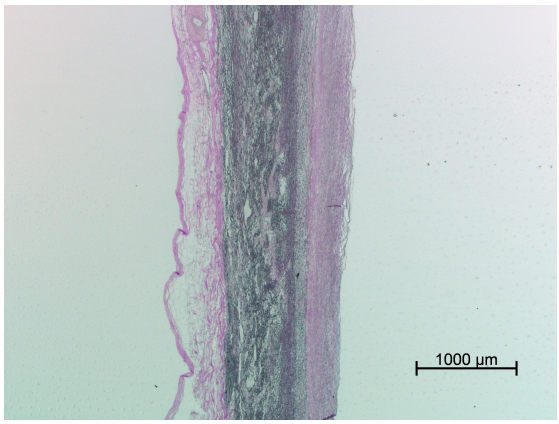

(a) Elastica van Gieson staining

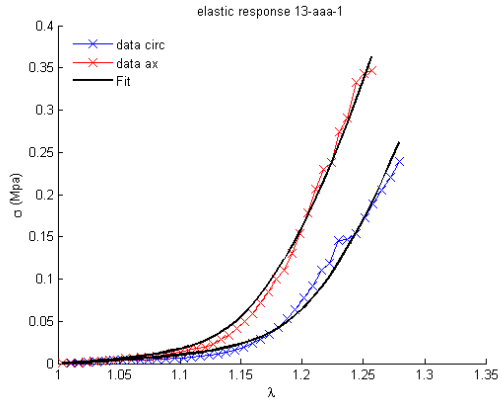

(b) Fitted elastic response

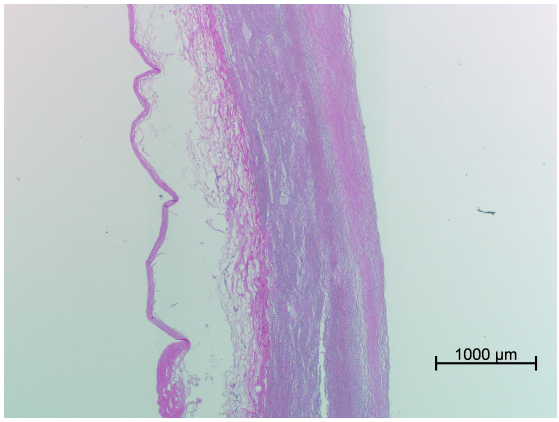

(c) Hematoxylin and eosin staining

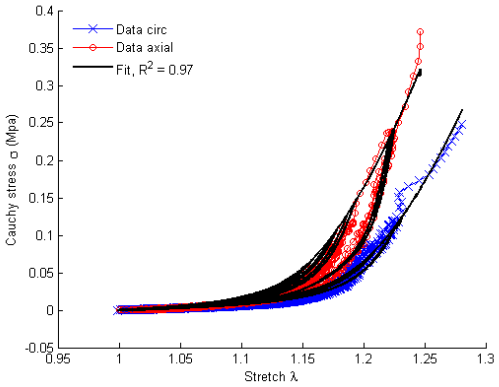

(d) Stress-strain response from mechanical testing and fitted response

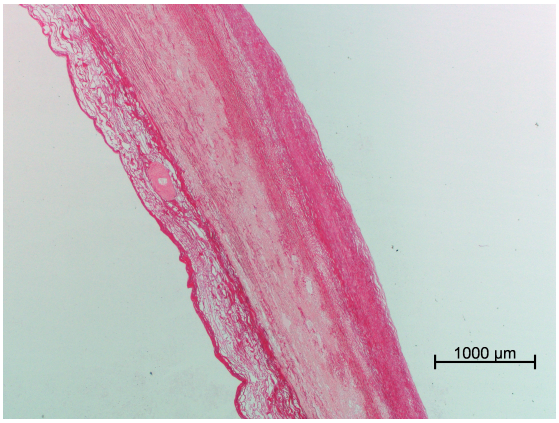

(e) Picosirius red staining

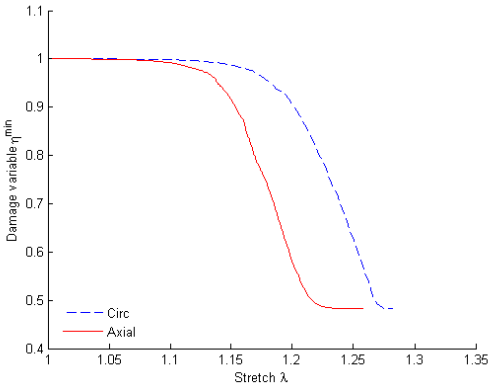

(f) Evolution of the damage variable vs. stretch

Figure C.13.: Sample T.2.2

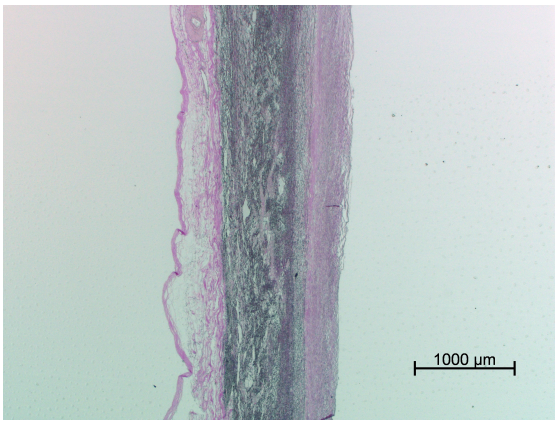

(a) Elastica van Gieson staining

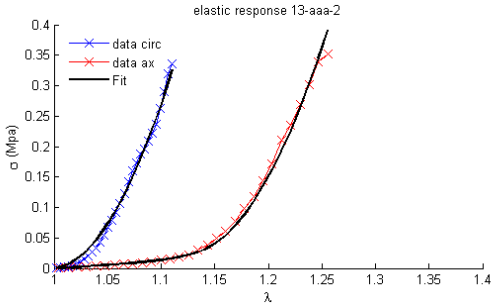

(b) Fitted elastic response

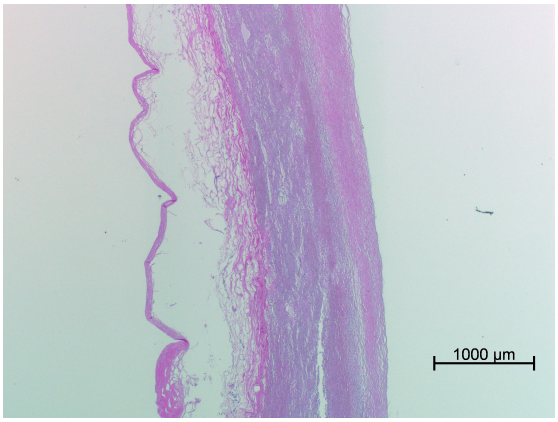

(c) Hematoxylin and eosin staining

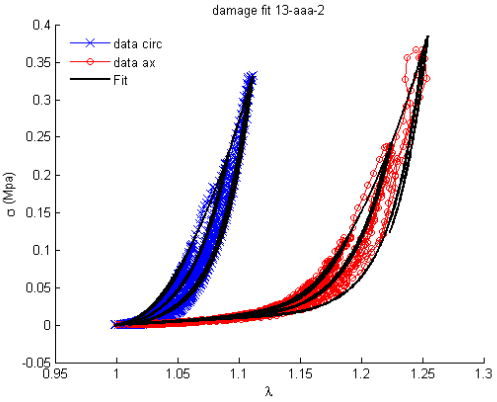

(d) Stress-strain response from mechanical testing and fitted response

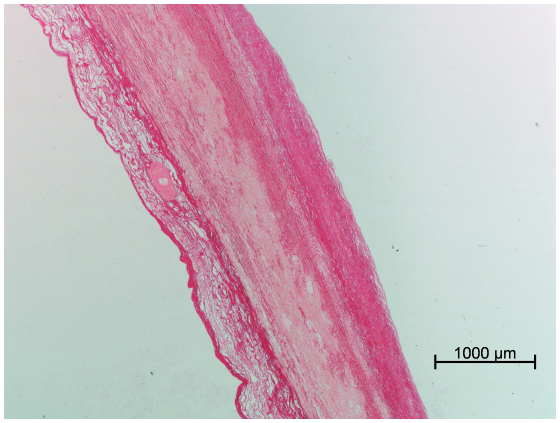

(e) Picosirius red staining

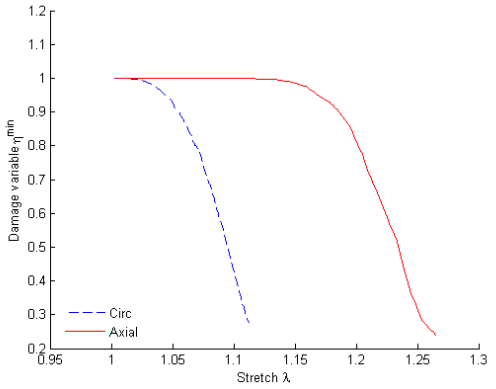

(f) Evolution of the damage variable vs. stretch

Figure C.14.: Sample T.3.1

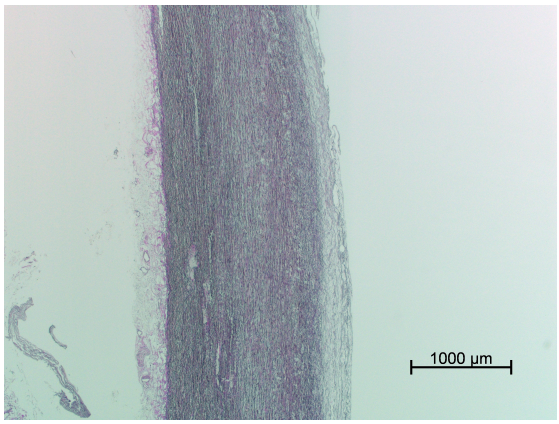

(a) Elastica van Gieson staining

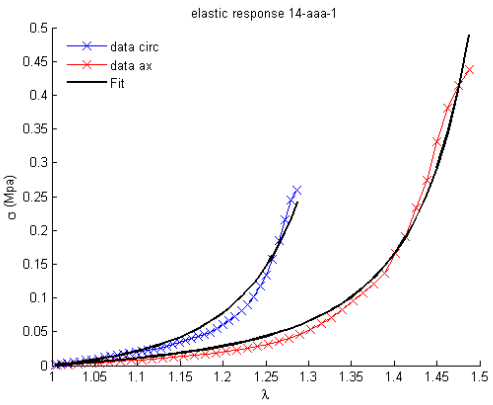

(b) Fitted elastic response

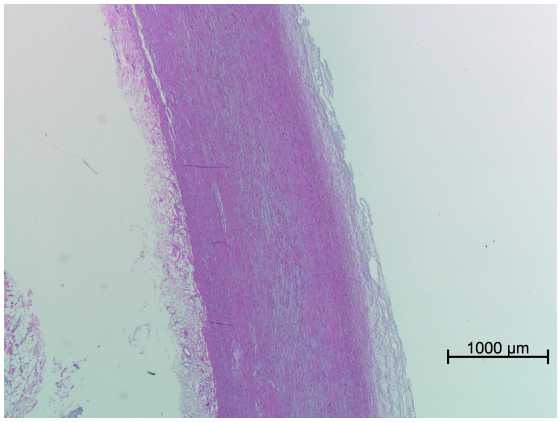

(c) Hematoxylin and eosin staining

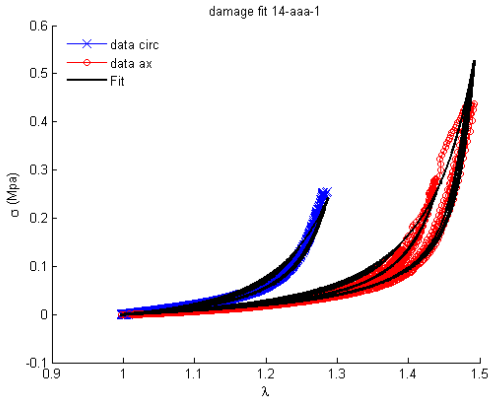

(d) Stress-strain response from mechanical testing and fitted response

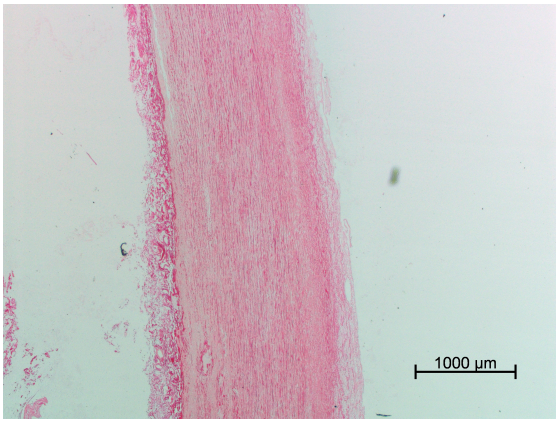

(e) Picosirius red staining

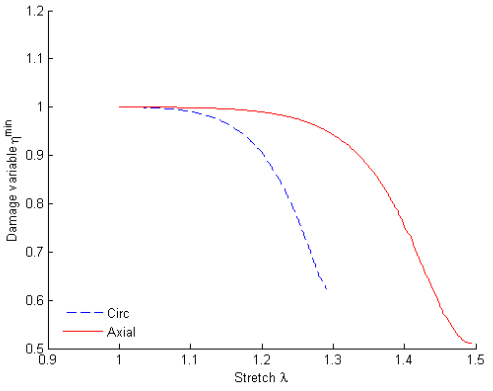

(f) Evolution of the damage variable vs. stretch

Figure C.15.: Sample T.3.2

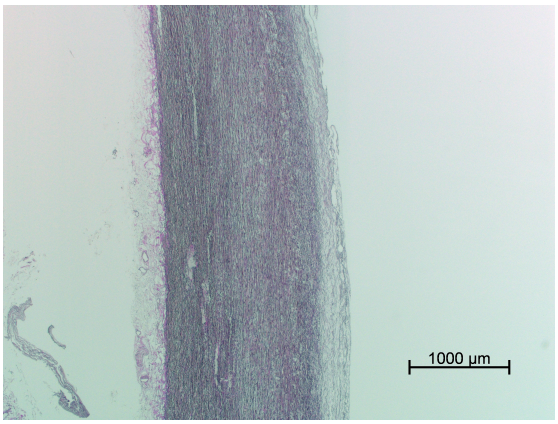

(a) Elastica van Gieson staining

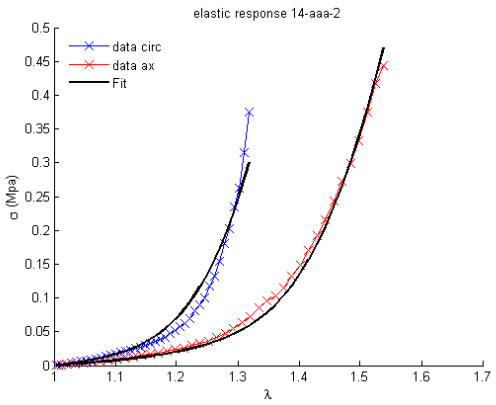

(b) Fitted elastic response

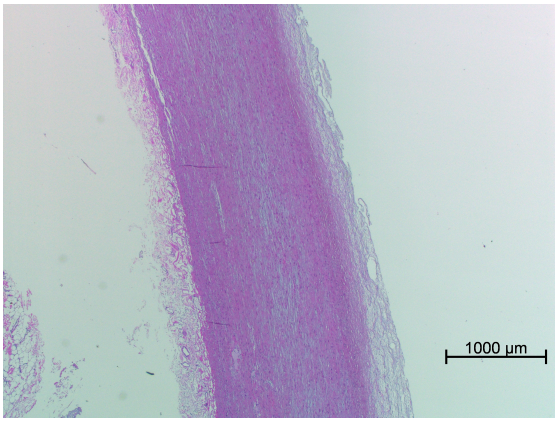

(c) Hematoxylin and eosin staining

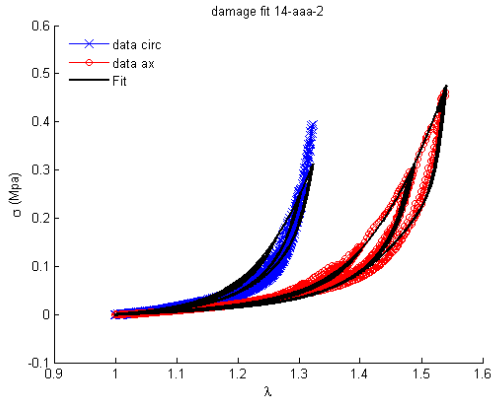

(d) Stress-strain response from mechanical testing and fitted response

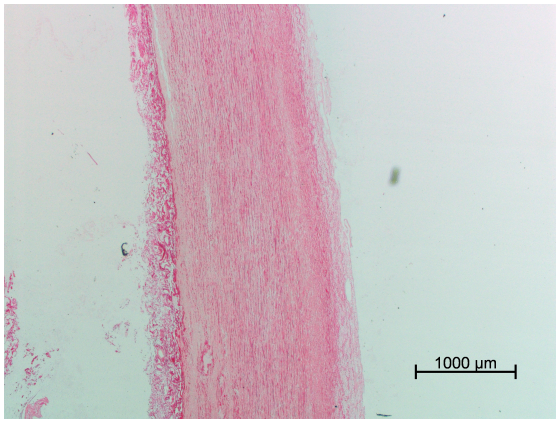

(e) Picosirius red staining

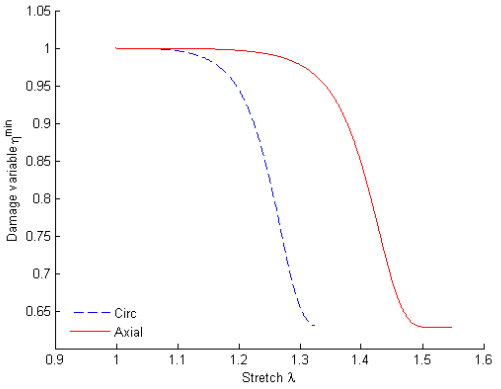

(f) Evolution of the damage variable vs. stretch

Figure C.16.: Sample T.4.1

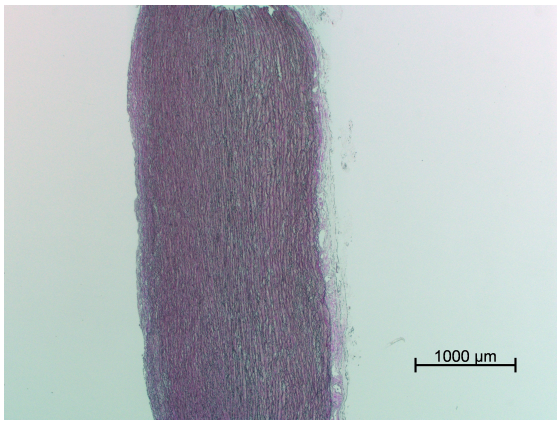

(a) Elastica van Gieson staining

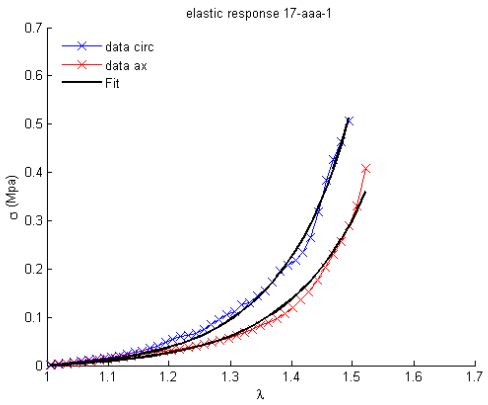

(b) Fitted elastic response

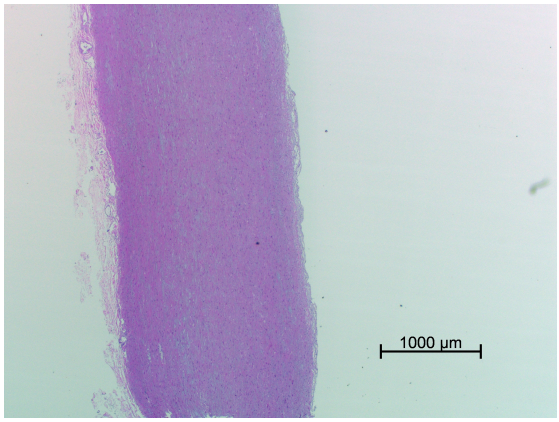

(c) Hematoxylin and eosin staining

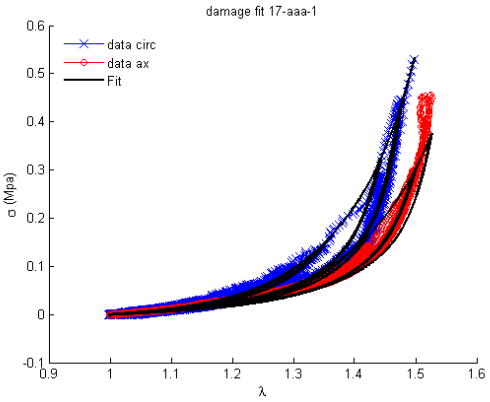

(d) Stress-strain response from mechanical testing and fitted response

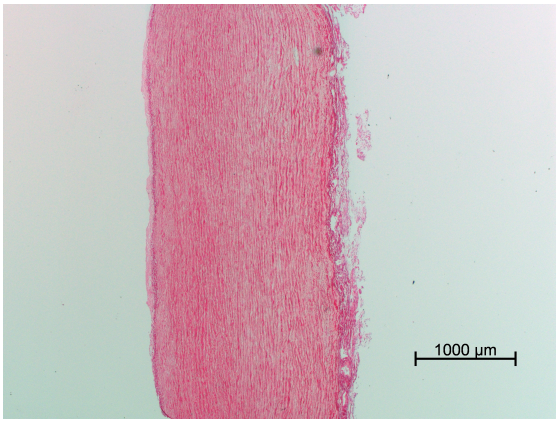

(e) Picosirius red staining

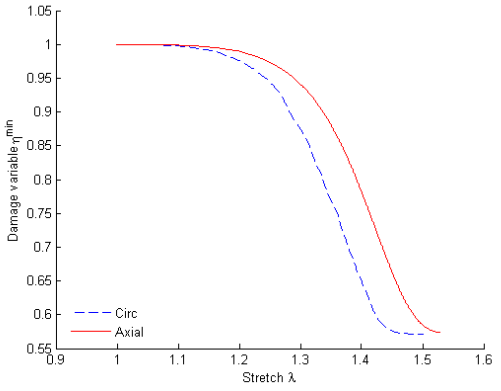

(f) Evolution of the damage variable vs. stretch

Figure C.17.: Sample T.4.2

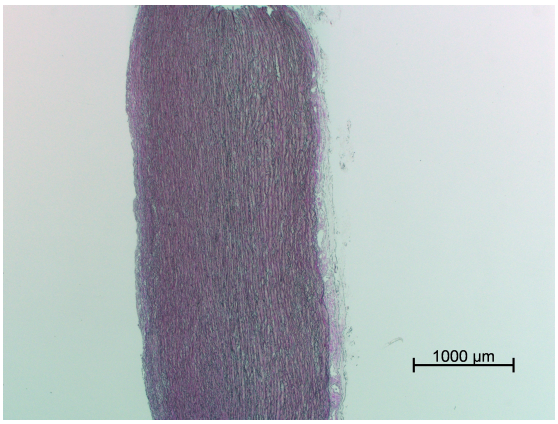

(a) Elastica van Gieson staining

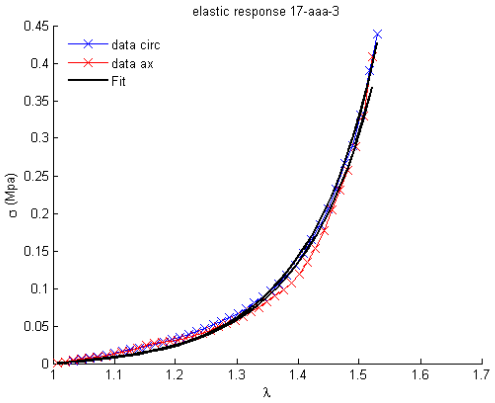

(b) Fitted elastic response

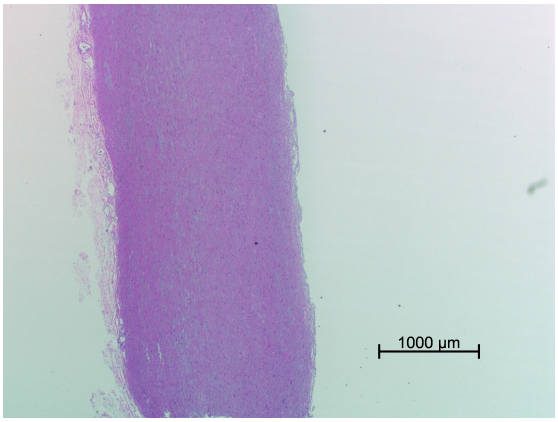

(c) Hematoxylin and eosin staining

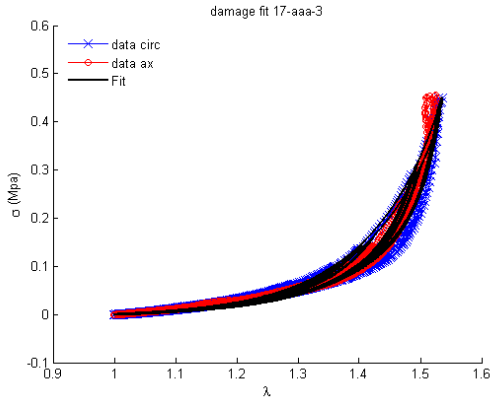

(d) Stress-strain response from mechanical testing and fitted response

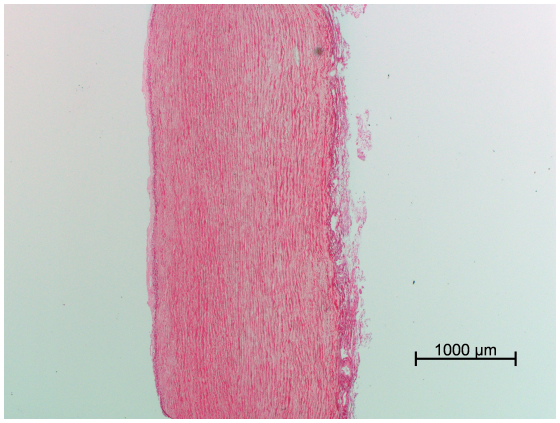

(e) Picosirius red staining

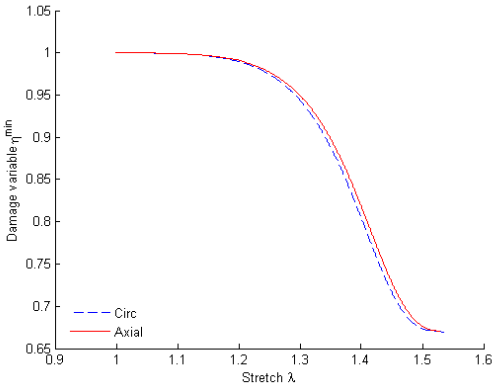

(f) Evolution of the damage variable vs. stretch

Figure C.18.: Sample T.5.1

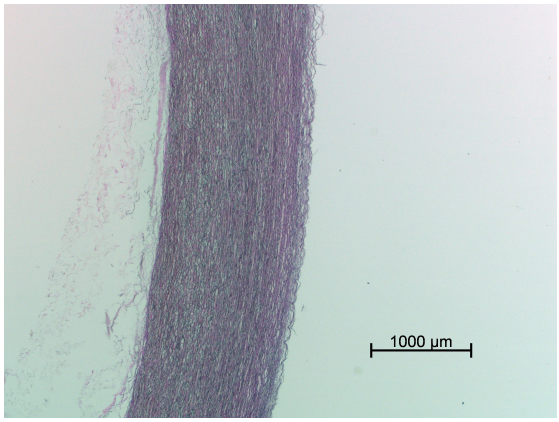

(a) Elastica van Gieson staining

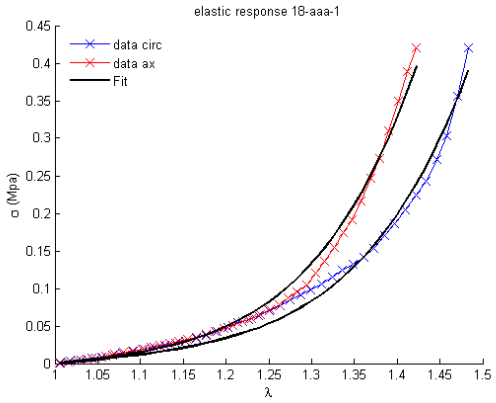

(b) Fitted elastic response

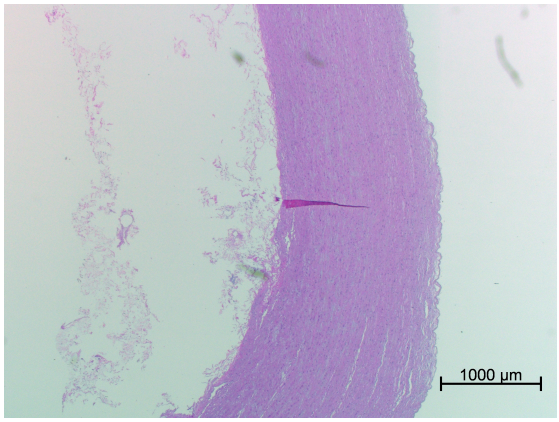

(c) Hematoxylin and eosin staining

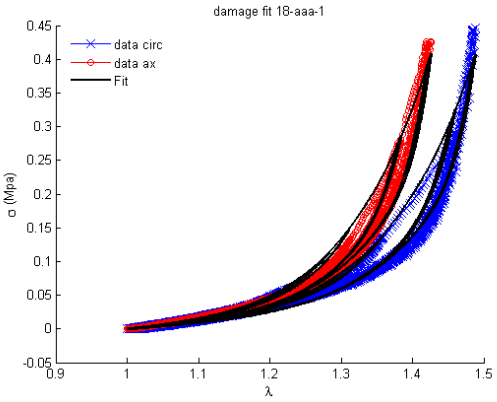

(d) Stress-strain response from mechanical testing and fitted response

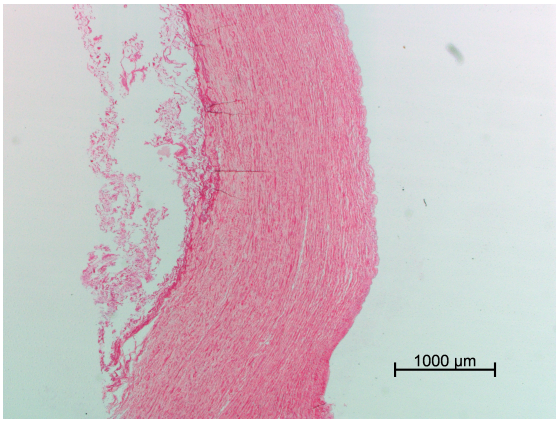

(e) Picosirius red staining

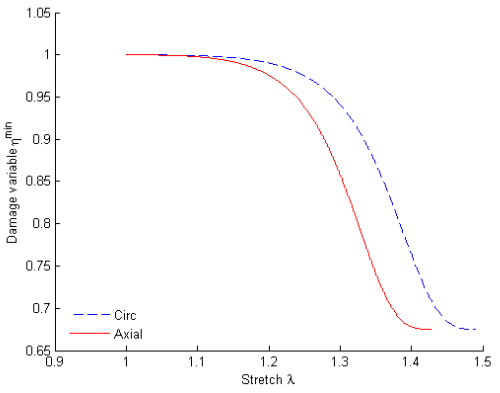

(f) Evolution of the damage variable vs. stretch

Figure C.19.: Sample T.5.2

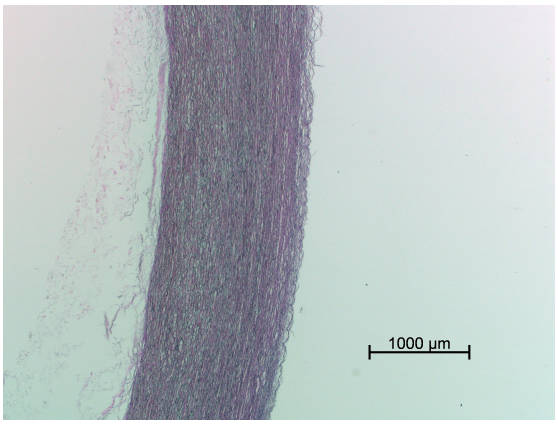

(a) Elastica van Gieson staining

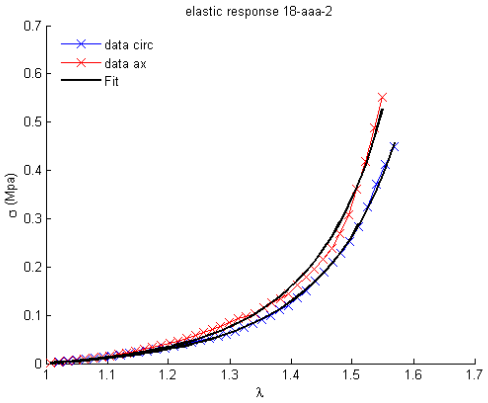

(b) Fitted elastic response

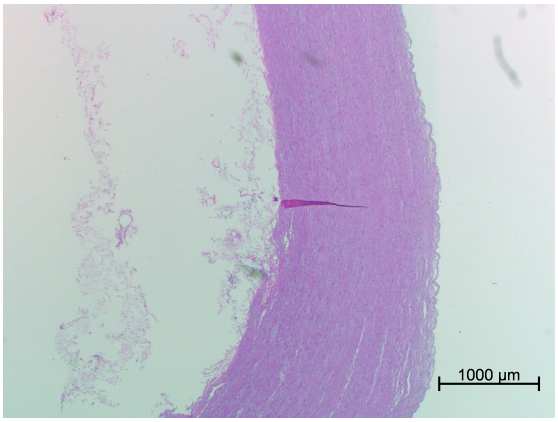

(c) Hematoxylin and eosin staining

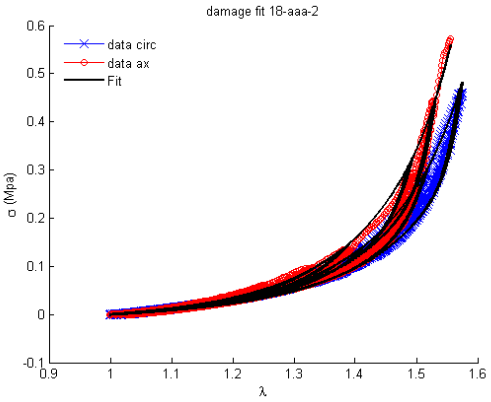

(d) Stress-strain response from mechanical testing and fitted response

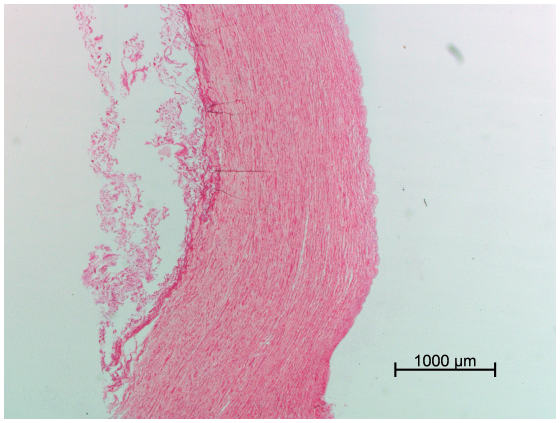

(e) Picosirius red staining

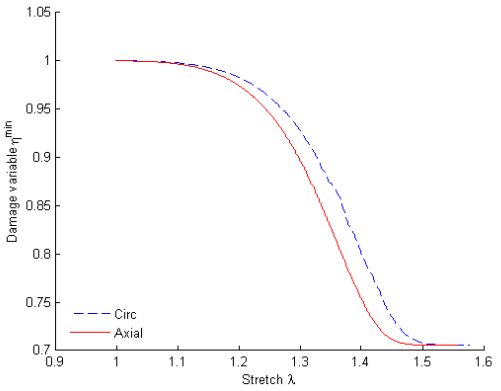

(f) Evolution of the damage variable vs. stretch

Figure C.20.: Sample T.6

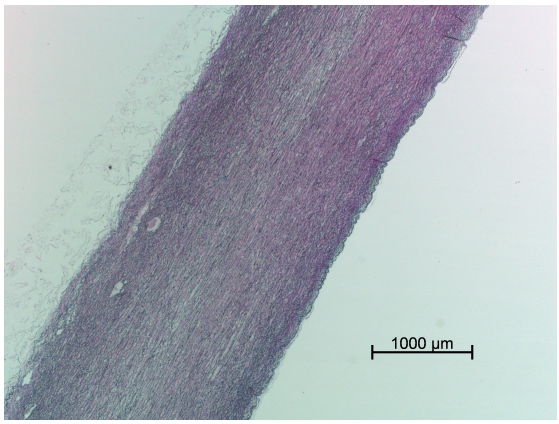

(a) Elastica van Gieson staining

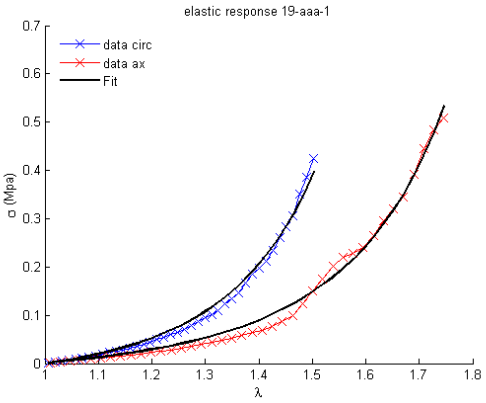

(b) Fitted elastic response

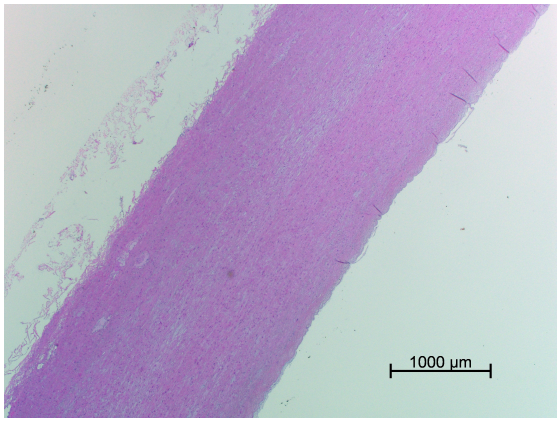

(c) Hematoxylin and eosin staining

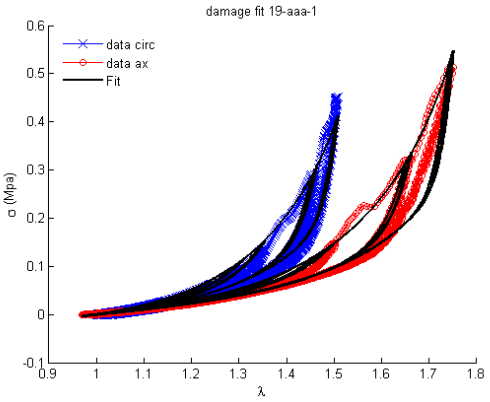

(d) Stress-strain response from mechanical testing and fitted response

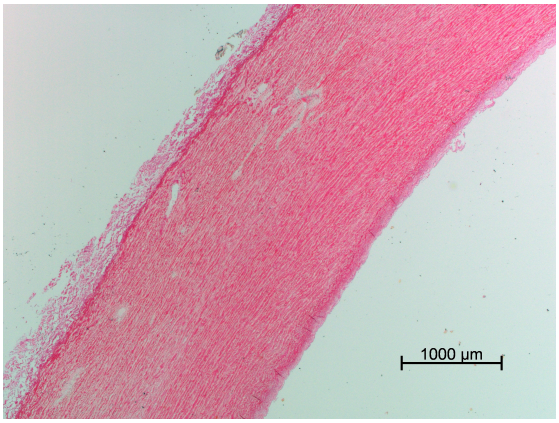

(e) Picosirius red staining

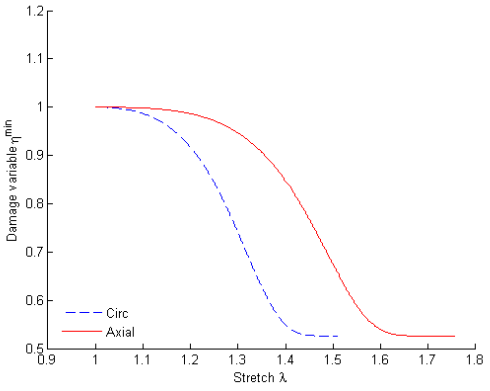

(f) Evolution of the damage variable vs. stretch